Tropomodulin1 is required for membrane skeleton organization and hexagonal geometry of fiber cells in the mouse lens

Roberta B. Nowak,[1] Robert S. Fischer,[1] Rebecca K. Zoltoski,[2] Jerome R. Kuszak,[3] and Velia M. Fowler[1]

[1]Department of Cell Biology, The Scripps Research Institute, La Jolla, CA 92037
[2]Department of Biological Health Sciences, Illinois College of Optometry, Chicago, IL 60616
[3]Departments of Pathology and Ophthalmology, Rush University Medical Center, Chicago, IL 60612

Hexagonal packing geometry is a hallmark of close-packed epithelial cells in metazoans. Here, we used fiber cells of the vertebrate eye lens as a model system to determine how the membrane skeleton controls hexagonal packing of post-mitotic cells. The membrane skeleton consists of spectrin tetramers linked to actin filaments (F-actin), which are capped by tropomodulin1 (Tmod1) and stabilized by tropomyosin (TM). In mouse lenses lacking Tmod1, initial fiber cell morphogenesis is normal, but fiber cell hexagonal shapes and packing geometry are not maintained as fiber cells mature. Absence of Tmod1 leads to decreased γTM levels, loss of F-actin from membranes, and disrupted distribution of β2-spectrin along fiber cell membranes. Regular interlocking membrane protrusions on fiber cells are replaced by irregularly spaced and misshapen protrusions. We conclude that Tmod1 and γTM regulation of F-actin stability on fiber cell membranes is critical for the long-range connectivity of the spectrin–actin network, which functions to maintain regular fiber cell hexagonal morphology and packing geometry.

Introduction

Regulation of epithelial cell hexagonal shape and packing geometry is a key feature of morphogenetic movements of epithelial sheets during development, and of planar cell polarity signaling that controls directional orientation of cells and their sensory organelles in tissues (Pilot and Lecuit, 2005; Green and Davidson, 2007; Jones and Chen, 2007; Lecuit and Lenne, 2007; Zallen, 2007). Genetic and computational modeling studies in developing epithelia from *Drosophila* have shown that cellular packing geometry depends on cell proliferation, the strength of cell–cell adhesions, and on actomyosin contractile activity in the cell cortex (Carthew, 2005; Gibson et al., 2006; Farhadifar et al., 2007; Käfer et al., 2007; Lecuit and Lenne, 2007; Cavey et al., 2008; Rauzi et al., 2008). These forces are regulated and balanced to control the extent of cell contacts and tension along lateral membranes, thereby maintaining or modulating cell shapes and hexagonal packing. Although actin assembly has been implicated in these processes, the role of actin filament (F-actin) organization and stability in hexagonal packing geometry of epithelial cells is relatively unexplored.

Spectrin, along with short F-actin and accessory proteins form a highly cross-linked network, referred to as the membrane skeleton, which underlies the inner surface of plasma membranes of metazoan cells (Luna and Hitt, 1992; Bennett and Baines, 2001). The membrane skeleton is linked to cell adhesion receptors and ion pumps and channels, and organizes sub-domains of the plasma membrane by virtue of the network's long-range connectivity (Bennett and Baines, 2001; Dubreuil, 2006; Bennett and Healy, 2008). The structural basis for long-range connectivity of the network is readily evident in expanded preparations of the erythrocyte membrane skeleton where it appears as a regular, quasi-hexagonal network in which the vertices of the network are short F-actins and the strands are long, flexible spectrin tetramers (Byers and Branton, 1985; Liu et al., 1987). In erythrocytes, the membrane skeleton controls cell

Correspondence to Velia M. Fowler: velia@scripps.edu

Abbreviations used in this paper: CAD, computer-assisted drawing; HBE, human bronchiole epithelial; SEM, scanning electron microscopy; TM, tropomyosin; Tmod, tropomodulin.

The Rockefeller University Press $30.00
J. Cell Biol. Vol. 186 No. 6 915–928
www.jcb.org/cgi/doi/10.1083/jcb.200905065

shapes, membrane stability, and deformability in the circulation (Mohandas and Evans, 1994; Bennett and Baines, 2001; Mohandas and Gallagher, 2008).

Emerging evidence also suggests a role for the spectrin-based membrane skeleton in influencing epithelial cell shapes and mechanical properties. Spectrins and their membrane linker proteins, ankyrins, are important for the biogenesis and maintenance of the characteristic tall shapes of polarized epithelial cells in culture (Kizhatil and Bennett, 2004; Kizhatil et al., 2007b) and for morphogenesis of epithelial cells in the mouse blastocyst (Kizhatil et al., 2007a). Mutations in α- or β-spectrins interfere with epidermal cell shape changes that contribute to the lengthening of the embryo in *Caenorhabditis elegans* (Moorthy et al., 2000; Praitis et al., 2005), as well as with morphogenesis of the follicular cell epithelium and the cuprophilic cells in the midgut epithelium of *Drosophila* (Thomas, 2001). Although many studies have addressed the functions of α- and β-spectrins and their linkers, the role of F-actin in the membrane skeleton and in epithelial morphogenesis in vivo is not understood. A priori, polymerization and stability of the F-actin linkers is expected, but not proven, to be critical for the network's long-range connectivity and functions (Gilligan and Bennett, 1993; Fowler, 1996).

The stereotyped program of vertebrate lens fiber cell morphogenesis provides a unique system to study epithelial hexagonal packing geometry in an organ in vivo. At the equator of the lens, epithelial cells differentiate to form lens fiber cells, which elongate more than 1,000-fold to extend from the anterior to the posterior of the lens (Fig. 1 A) (Kuszak et al., 1996; McAvoy et al., 1999; Zelenka, 2004). In the mouse lens, similar to the human, fiber cells curve as they elongate, forming offset Y-shaped suture patterns at the anterior and posterior (Fig. 1, A and C; Fig. S1) (Kuszak et al., 2004a,b, 2006). The elongated fiber cells are arranged as a series of concentric layers or sheets, in which the cross-sectional profiles of cells appear as flattened hexagons oriented along the lens circumference (Fig. 1 B) (Bassnett and Winzenburger, 2003; Kuszak et al., 2004a). After new fiber cells are added at the periphery during lens growth, they are displaced inward so that the youngest cells are at the periphery and older, more mature cells are more centrally located (Kuszak et al., 1996; McAvoy et al., 1999; Zelenka, 2004). As cells move inwards, they eventually lose their nuclei and other organelles to form the organelle-free zone, or lens nucleus (Bassnett, 2009). Thus, equatorial sections of the lens reveal a timeline of fiber cell morphogenesis and maturation laid out radially, from the outside in (Bassnett and Winzenburger, 2003; Blankenship et al., 2007; Bassnett, 2009). Spectrin, ankyrin, and other membrane skeleton components are associated with lens fiber cell membranes (Nelson et al., 1983; Allen et al., 1987; Faquin et al., 1988; Kaiser et al., 1989; Lee et al., 2000; Moré et al., 2001; Straub et al., 2003), presenting an opportunity to investigate how actin dynamics in the membrane skeleton contributes to hexagonal packing geometry in vivo.

F-actin stability depends on capping proteins at filament ends that prevent assembly and disassembly, and on tropomyosins (TMs) that bind along the sides of filaments, blocking severing and reducing subunit dissociation (Pollard et al., 2000; Cooper, 2002; Gunning et al., 2005). Tropomodulins (Tmods) are actin pointed end-capping proteins that bind to TMs and cap TM-coated F-actin with high affinity, preventing polymerization and depolymerization, thereby regulating filament lengths

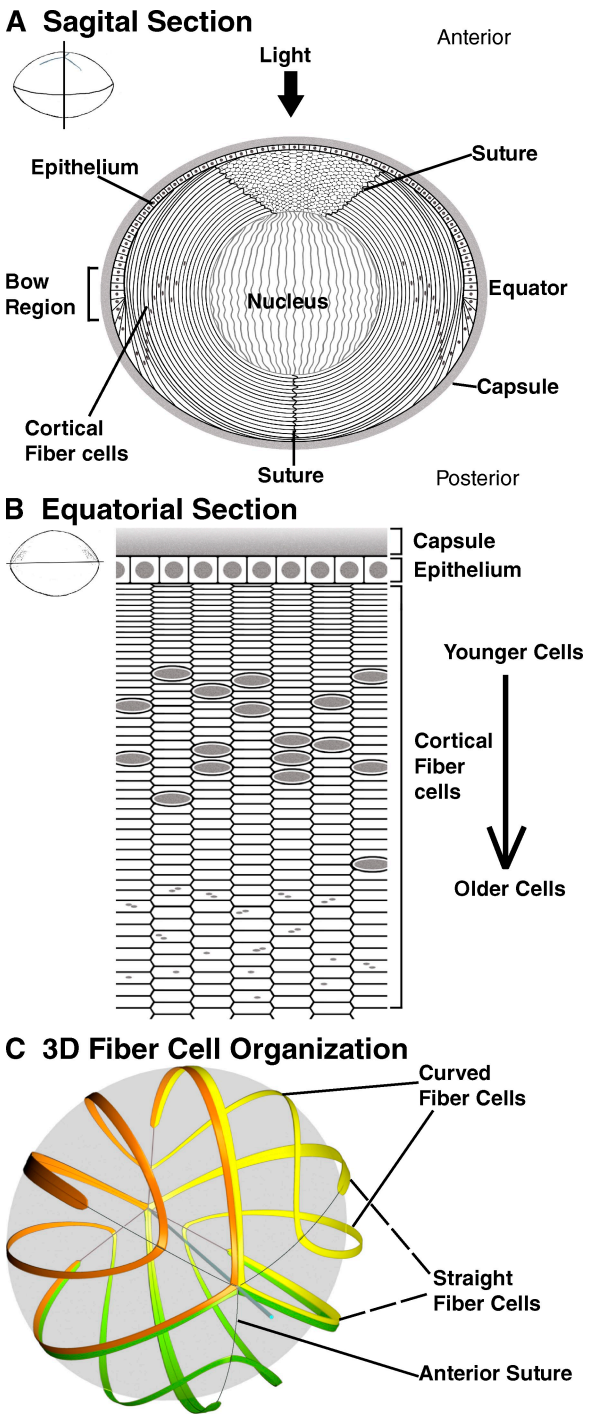

Figure 1. **Diagrams of mouse lens epithelial and fiber cell organization.** (A) Sagittal and (B) equatorial sections of the mouse lens. (C) 3D-CAD reconstruction of selected fiber cells in the mouse lens, modified from Kuszak et al. (2006). Fiber cells are curved so that their ends contact one another at the offset Y-shaped sutures at the anterior and posterior of the lens. In A, note that fiber cell cross sections are visible between the two anterior suture branches in a sagittal section. Gray ovals or circles, cell nuclei. Gray dots, nuclear remnants. In C, Y-shaped sutures are indicated by thin gray lines. See Fig. S1 for a stereo pair of C.

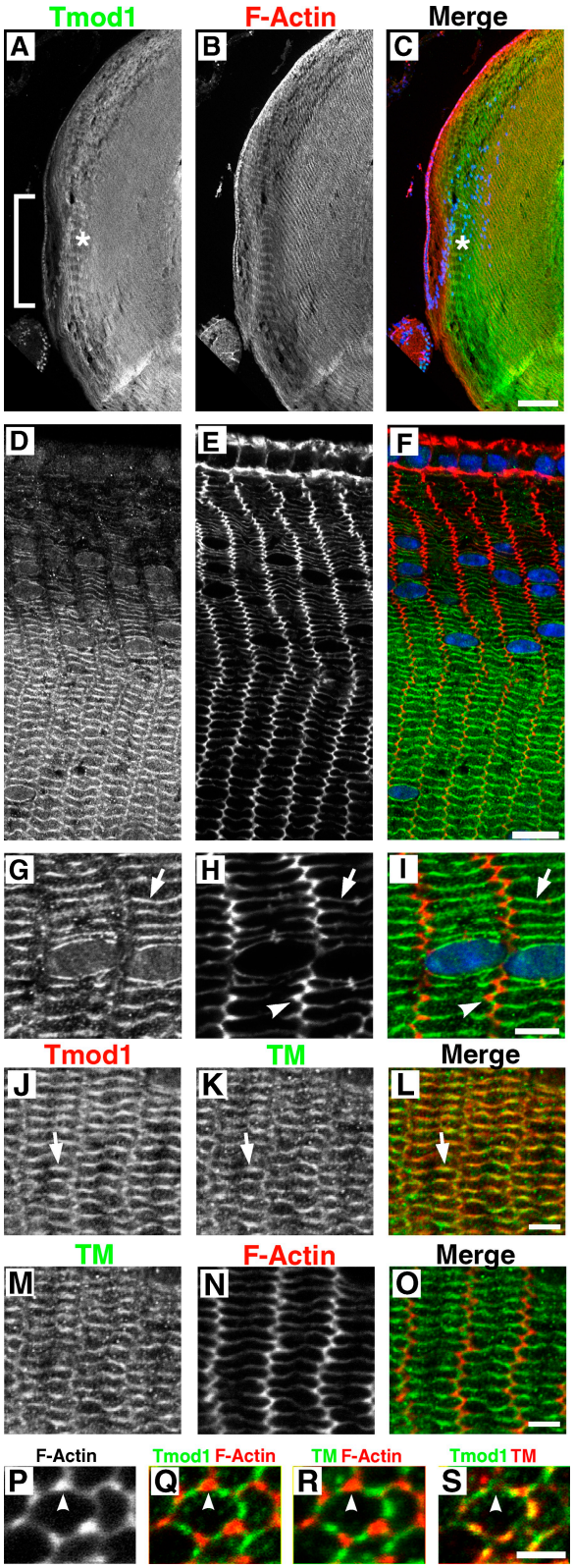

Figure 2. **Tmod1 assembles with TM on broad and narrow sides of fiber cell membranes as they mature and are displaced inwards.** (A–C) Sagittal or (D–O) equatorial sections of 1-mo-old *Tmod1+/+$^{Tg+}$* mouse lenses stained for (A–I) Tmod1, F-actin, and nuclei (blue in merges); or (J–O) Tmod1, TM, and F-actin. (P–S) Sagittal section of P15 lens showing a stretched fiber cell cross section near the anterior suture (Fig. 1), stained for Tmod1, TM, and F-actin. Bracket, bow region; asterisk, maturing fiber cells; arrows, fiber cell broad sides; arrowheads, fiber cell vertices. Bars: (A–C) 114 µm; (D–F) 11 µm; (G–O) 4 µm; (P–S) 5 µm.

and imparting stability (Weber et al., 1994; Fowler, 1996; Fischer and Fowler, 2003). Tmods were first discovered in human erythrocytes, where Tmod1 caps the short TM–F-actin in the membrane skeleton (Fowler, 1987, 1990, 1996). Tmod1 (Tmod4 in chickens) is also associated with the membrane skeleton in the lens, where it is up-regulated upon fiber cell differentiation, assembles, and remains associated with fiber cell membranes as they mature (Woo and Fowler, 1994; Sussman et al., 1996; Fischer et al., 2000; Lee et al., 2000, 2001). Targeted deletion of *Tmod1* in mice results in failure of myofibril assembly and aborted cardiac development, leading to embryonic lethality at E9.5 (Chu et al., 2003; Fritz-Six et al., 2003), before the lens develops (McAvoy et al., 1999).

We generated a viable *Tmod1* knock-out mouse by expressing Tmod1 only in the heart (McKeown et al., 2008), which has allowed us to determine the in vivo function of Tmod1 in the lens. Our studies reveal that initial fiber cell morphogenesis in lenses without Tmod1 is normal, but fiber cell shapes become abnormal and their hexagonal packing geometry is lost subsequently, as fiber cells mature in the lens cortex. Biochemical and morphological analyses show that Tmod1 stabilization of γTM on F-actin in the membrane skeleton is critical for the organization and connectivity of the spectrin–actin network, the morphologies of fiber cell membrane protrusions, and for maintenance of hexagonal geometry. The spectrin–actin network may provide a uniformly distributed elastic tension along the membrane, counterbalancing cell–cell adhesion and actomyosin contractile forces, thereby providing a novel control point to achieve and maintain hexagonal packing symmetry of epithelial cells.

Results

Tmod1 assembles with TM on broad and narrow sides of maturing fiber cell membranes

To investigate Tmod1 assembly in lens fiber cell morphogenesis, we used immunofluorescence staining and confocal microscopy to localize Tmod1 in sagittal and equatorial cryosections of 1-mo-old mouse lenses. Tmod1 protein is barely detected in the epithelial cells or in newly differentiated, elongating fiber cells located in the bow region (Fig. 2, A [bracket] and D), whereas F-actin staining is comparable in both epithelial and fiber cells (Fig. 2, B and E). Strikingly, Tmod1 staining increases dramatically in somewhat older cortical fiber cells located ∼40–50 µm away from the epithelium (Fig. 2, A [asterisk] and D; Fig. S2). As shown previously in the chicken lens for Tmod4 (Lee et al., 2000), Tmod1 staining in the mouse lens remains high as cells are displaced inwards, even in the inner fiber cells that have lost their nuclei in the organelle-free zone (Fig. 2, A and C; Fig. S2). Strikingly, Tmod1 assembles preferentially on the membranes forming the broad and narrow sides of the fiber cells, which appear as the long and short sides of the flattened hexagons in these 2D images of fiber cell cross sections (Fig. 2, D and F; G and I [arrow]). This pattern contrasts with F-actin, which is present along the entire fiber cell membrane, but is enriched at the vertices of the flattened hexagons as

compared with Tmod1 (Fig. 2, E, F, H, and I [arrowheads]). Mouse lens TM is present in a similar pattern as Tmod1, co-localizing predominantly with Tmod1 on the broad and narrow sides of fiber cells (Fig. 2, J–L), and not with the bright F-actin dots at the vertices (Fig. 2, M–O). This is particularly evident in cross sections of the anterior portions of individual fiber cells that were stretched during sectioning, revealing that both Tmod1 and TM are localized in the middles of the sides between the vertices (Fig. 2, P–S). These data indicate that Tmod1 assembles subsequent to initial fiber cell morphogenesis, and is associated with TM and F-actin in membrane domains located on the broad and narrow sides of fiber cells.

Lenses develop normally but fiber cell packing is disordered in the absence of Tmod1

To investigate the function of Tmod1 in lens fiber cell organization in the mouse lens, we studied lenses from viable *Tmod1* null animals expressing a *Tmod1* transgene in the heart under the control of the α-myosin heavy chain promoter (*Tg(αMHC-Tmod1)*) (McKeown et al., 2008). With the exception of the heart (McKeown et al., 2008), $Tmod1-/-^{Tg(\alpha MHC\text{-}Tmod1)}$ mice have no detectable Tmod1 protein in the lens (Fig. 3 A) or in any other tissues (unpublished data). The amount of Tmod1 protein in lenses from *Tmod1+/−* mice is equivalent to lenses from *Tmod1+/+* mice, regardless of the presence or absence of the *αMHC-Tmod1* transgene (Fig. 3 A and Fig. S3). Total levels of actin, crystallins, and other abundant lens proteins are unaffected by the absence of Tmod1 or by the transgene (Fig. 3 A). For simplicity, $Tmod1+/+^{Tg(\alpha MHC\text{-}Tmod1)}$ and $Tmod1-/-^{Tg(\alpha MHC\text{-}Tmod1)}$ genotypes will be referred to as $Tmod1+/+^{Tg+}$ and $Tmod1-/-^{Tg+}$. Dissection of lenses from $Tmod1+/+^{Tg+}$ and $Tmod1-/-^{Tg+}$ mice of various ages from 1 mo to 1 yr showed that lenses were transparent with no cataracts in the absence of Tmod1 (Fig. 3 B and unpublished data). Measurements of lens weights and sizes also showed that lens growth was normal in the absence of Tmod1 (Fig. 3, C and D). Examination of lens morphology in sagittal sections of lenses from E16.5, P13, 1-mo-old, or adult animals further demonstrated that epithelial cell organization, initial fiber cell morphogenesis, and subsequent nuclear loss were similar in the presence and absence of Tmod1 (Fig. S2; see Fig. 5; unpublished data). Thus, the absence of Tmod1 does not lead to perturbations of initial events of fiber cell differentiation, elongation, and migration, or in overall lens development and growth.

However, inspection of cortical fiber cell packing organization in equatorial cryosections of lenses from P13 to 1-mo-old mice revealed that patches of disordered fiber cells were frequently observed in $Tmod1-/-^{Tg+}$ lenses, as compared with the hexagonal packing geometry of fiber cells in $Tmod1+/+^{Tg+}$ lenses, which rarely exhibit disordered regions (Fig. 4, A–F). In these regions, instead of exhibiting regular, flattened hexagonal shapes with brightly stained F-actin at their vertices (Fig. 4, A, B, and E), fiber cell shapes in the absence of Tmod1 were polygonal and often somewhat rounded, with variable numbers of vertices per cell and irregular lengths of connecting membranes

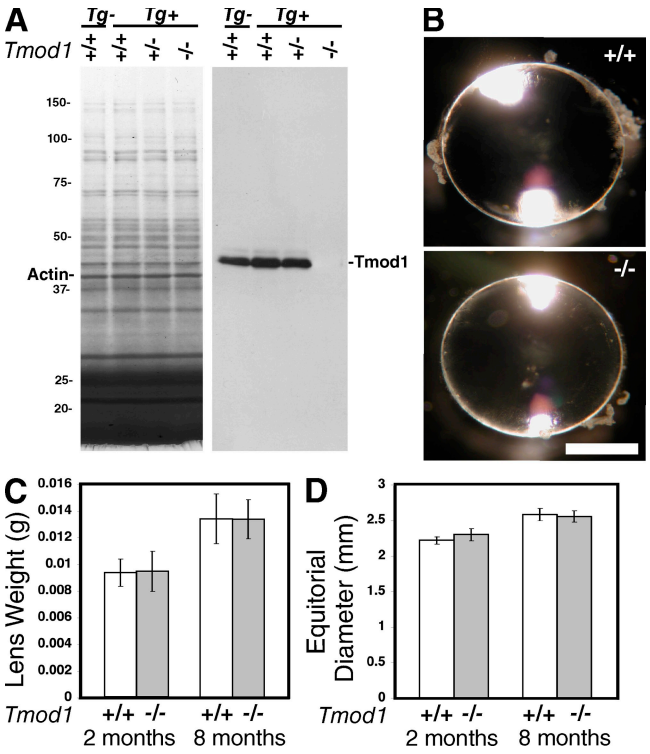

Figure 3. **Mouse lenses lacking Tmod1 grow normally and are transparent.** (A) Ponceau S staining (left) and Western blot (right) of total lens extracts from 4-mo-old mice. (B) Dissected lenses from 4-mo-old mice viewed in oblique illumination. Bar, 1 mm. (C) Weights and (D) equatorial diameters for lenses from 2- and 8-mo-old mice are not affected by absence of Tmod1. At 2 mo, *n* = 8 lenses for each genotype. At 8 mo, *n* = 20 for $Tmod1+/+^{Tg+}$ and 15 for $Tmod1-/-^{Tg+}$.

(Fig. 4, C, D, and F). The presence of disordered cell packing was sporadic, often extending across many radial columns of fiber cells and in other cases involving only a few disordered cells adjacent to normal regions of fiber cells in $Tmod1-/-^{Tg+}$ lenses (Fig. 4, C and D). At the equator, regions displaying disordered fiber cell packing tended to be located 20–30 cell layers in from the epithelium (Fig. 4 C), in the region where Tmod1 normally assembles on membranes (Fig. 1). This indicates that absence of Tmod1 affects geometry of maturing fiber cells rather than initial elongation and organization. However, fiber cell disorder is not related to organelle and nuclear loss, based on the presence of Hoechst-stained nuclei in regions exhibiting disorder (Fig. 4, C, D, and F).

We quantified the changes in fiber cell organization in the absence of Tmod1 by comparison of variations in F-actin staining intensity along radial line scans in low magnification images of lens cryosections (Fig. 4, G and H). The line scans revealed an ∼1.6-fold greater variation from the average F-actin staining intensity in the absence than in the presence of Tmod1 (Fig. 4, I–K). This likely reflects misalignment and disorganization of the radial columns of fiber cells as well as inhomogeneity in F-actin distribution in the absence of Tmod1 (see Fig. 8), resulting in increased variation of intensity along a radial line. Visual inspection of the line scans also suggested that the degree of variation tended to increase from the periphery toward the inner cortex in the absence of Tmod1, but this was not

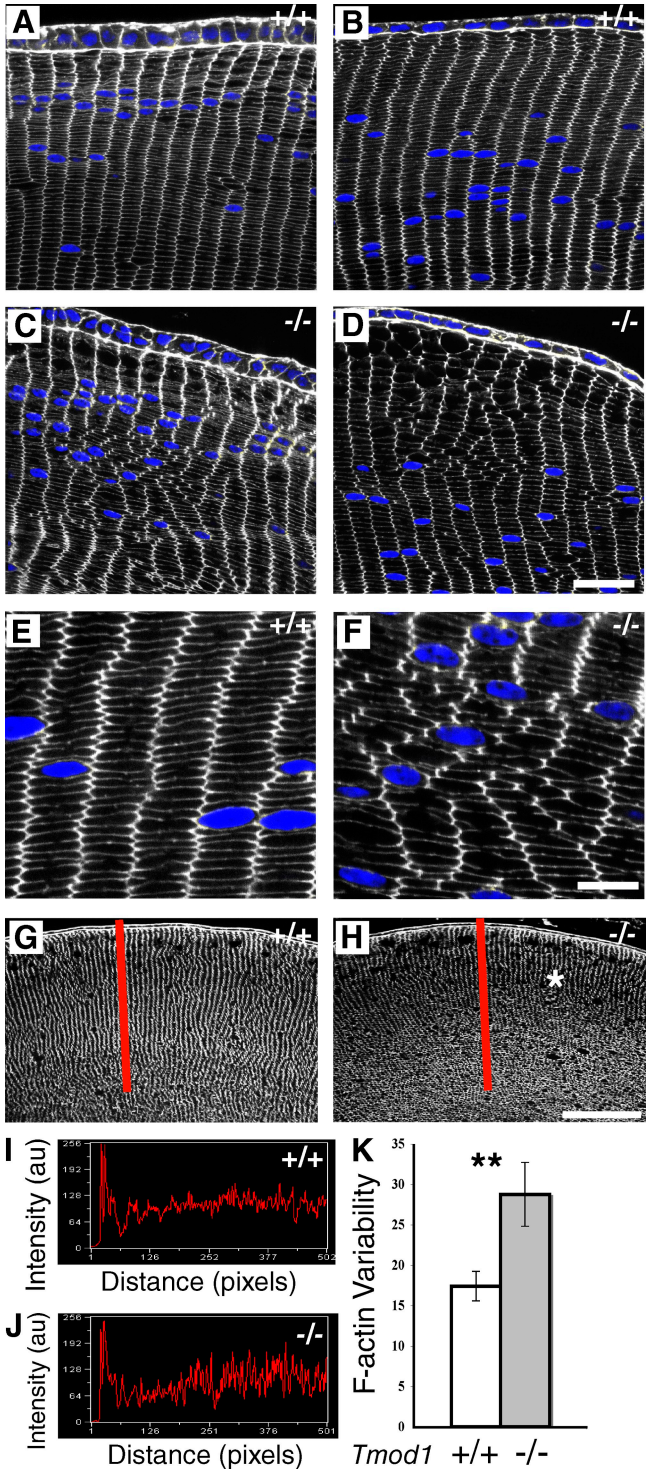

Figure 4. **Fiber cell hexagonal packing geometry and radial column organization is disturbed in the absence of Tmod1.** (A–F) Equatorial sections of 1-mo-old mouse lenses stained for F-actin and nuclei (blue). (G and H) Sagittal sections of the anterior region of P13 lenses stained for F-actin. (A, B, E, G, and I) *Tmod1+/+*$^{Tg+}$ and (C, D, F, H, and J) *Tmod1−/−*$^{Tg+}$ mice. (I and J) Representative line scans of F-actin fluorescence along the radial lines (red) in G and H. (K) Variability in F-actin intensity is ∼1.6-fold greater in absence of Tmod1 ($P < 0.0001$). $n = 10$ line scans from two sections per genotype. Bars: (A–D) 22 µm; (E and F) 8 µm; (G and H) 90 µm.

possible to quantify (Fig. 4, I and J). Interestingly, overall F-actin intensity in the peripheral region of the cortex appeared somewhat reduced in the absence of Tmod1 (Fig. 4 H, asterisk; and see Fig. 8).

To investigate whether defects in fiber cell shape and disordered packing in the absence of Tmod1 were present in adult lenses, we examined fiber cell morphologies in sections of lenses embedded in epoxy resin (Chung et al., 2007). Fiber cell geometry was evaluated in sagittal sections of the peripheral cortex, where Tmod1 is assembled on membranes of the anterior and posterior segments of the elongating fiber cells (Fig. 2 A). Cross-sectional profiles of fiber cells in the anterior hemisphere of *Tmod1+/+*$^{Tg+}$ lenses appear as identically sized chevrons regularly arranged in parallel, offset radial columns, resulting in hexagonal packing geometry (Fig. 5, B and G). In contrast, cortical fiber cells in *Tmod1−/−*$^{Tg+}$ lenses exhibit variable sizes and shapes, and are not arranged in precise radial columns (Fig. 5, E and H). Similar to lenses from younger, 1-mo-old animals (Fig. 4), patches of fiber cell disorder were adjacent to ordered regions in lenses from these adult animals, but cell shapes appeared distorted throughout (Fig. 5, E and H). Quantification of fiber cell organization by tracing the paths of the radial columns revealed very few branches in *Tmod1+/+*$^{Tg+}$ lenses (Fig. 5 C), whereas in *Tmod1−/−*$^{Tg+}$ lenses numerous branch points were present, where one fiber cell is on top of two other cells (Fig. 5 F). These data show that the radial columns branch ∼2.5-fold more frequently in the absence than in the presence of Tmod1, both at the anterior and posterior of the lens (Fig. 5 I). In conclusion, maintenance of fiber cell hexagonal shapes, packing geometry, and radial column organization in the lens cortex is compromised in the absence of Tmod1.

Fiber cell membrane morphologies and protrusions are abnormal in the absence of Tmod1

To investigate fiber cell membrane morphology at higher resolution, we performed scanning electron microscopy (SEM) of lens cortical "peels" (Sivak et al., 1994; Kuszak et al., 2004a) prepared from adult mice (Fig. 6). In *Tmod1+/+*$^{Tg+}$ lenses, the successive layers of flattened fiber cells are readily visible (Fig. 6 A), exhibiting regular rows of elaborate ∼3–4-µm paddle-like protrusions along their length (Fig. 6 B, arrow). These paddle-like protrusions contain rows of even smaller ∼0.5-µm protrusions, as described previously (Rafferty, 1985; Sivak et al., 1994; Kuszak et al., 2004a; Blankenship et al., 2007). In contrast, in *Tmod1−/−*$^{Tg+}$ lenses, fiber cells have a more tube-like rather than flattened shape, and regular layers of individual fiber cells are more difficult to distinguish (Fig. 6 C and unpublished data), presumably reflecting their disorganized packing and variable shapes (Figs. 4 and 5). At higher magnification, the paddles in *Tmod1−/−*$^{Tg+}$ lenses appear to lack the small protrusions, are misshapen with variable sizes, and are not arranged in regular rows (Fig. 6 D, arrow). Thus, the absence of Tmod1 leads to abnormal placement and morphologies of fiber cell membrane protrusions, which may contribute to altered cell–cell interactions, abnormal cell shapes, and disordered packing.

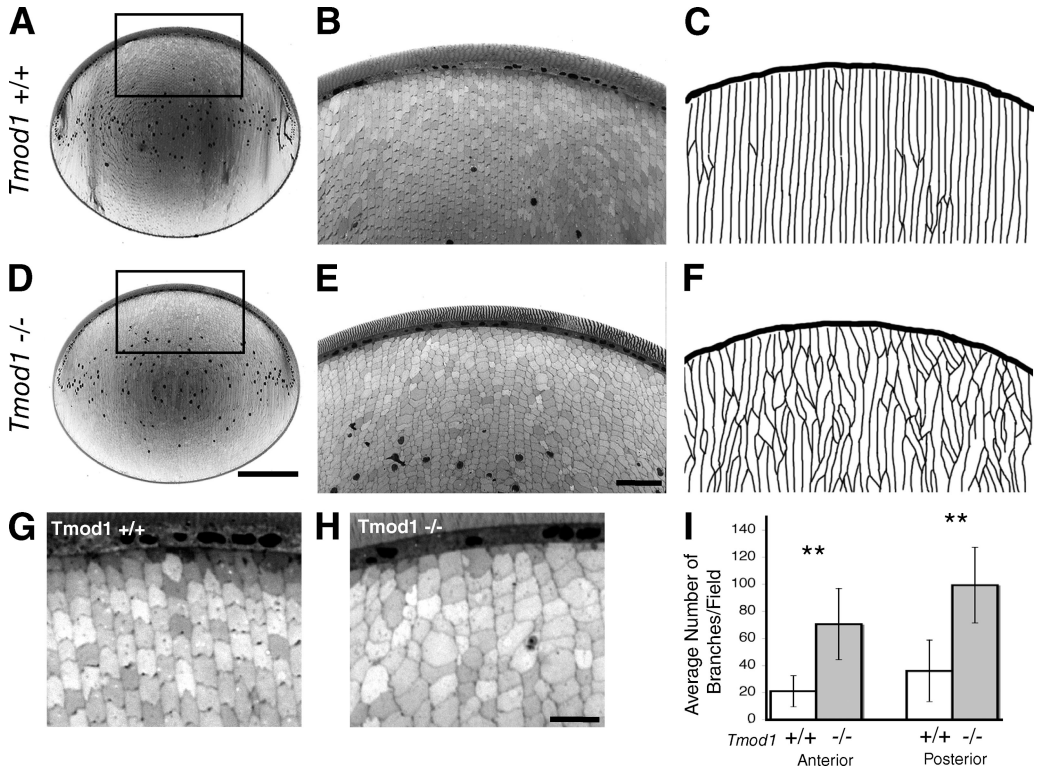

Figure 5. **Fiber cells in adult lenses lacking Tmod1 exhibit abnormal fiber cell shapes and sizes, disordered packing, and radial column organization.** Light micrographs of sagittal sections of lenses from 5-mo-old *Tmod1+/+*$^{Tg+}$ (A, B, and G) and *Tmod1−/−*$^{Tg+}$ (D, E, and H) mice. B and E are higher magnification views of boxed regions in A and D. (C and F) Tracings of fiber cell radial columns from B and E. (I) Numbers of column branches per field are ∼2.5-fold greater in the absence of Tmod1 ($P < 0.009$ for anterior; $P < 0.004$ for posterior). $n = 6$ *Tmod1+/+*$^{Tg+}$ mice (5–10 mo) and 6 *Tmod1−/−*$^{Tg+}$ mice (4–8 mo). Bars: (A and D) 500 µm; (B and E) 10 µm; (G and H) 20 µm.

In an effort to explore the relationship between Tmod1 and membrane protrusion morphology, we examined cross sections of fiber cells located ∼50 cells in from the epithelium, where the paddles form in wild-type lenses (Blankenship et al., 2007). In these regions, Tmod1 appears somewhat punctate on both broad and narrow membrane domains and does not completely overlap with F-actin, which is continuous along the curving membrane contours likely corresponding to the paddles and small protrusions (Fig. S4, A–C, arrows). In contrast, F-actin appears somewhat discontinuous in the comparable regions of *Tmod1−/−*$^{Tg+}$ lenses (Fig. S4 D), consistent with the altered paddle and protrusion morphology evident by SEM (Fig. 6). The presence of Tmod1 in the paddle regions, and perturbations in F-actin in the absence of Tmod1, support a function for Tmod1 in their morphogenesis and/or maintenance. However, the complex 3D geometries of the curving paddles and the small protrusion sizes (∼0.5 µm), which are below the axial resolution of confocal laser-scanning fluorescence microscopy (∼0.6 µm) (Gustafsson, 1999; Pawley, 2006), make it impossible to determine whether the Tmod1 is present within or between the small protrusions on the paddles.

A short γTM isoform on fiber cell membranes is reduced in the absence of Tmod1

Tmods enhance the association of TMs with F-actin pointed ends, reducing actin dynamics and stabilizing F-actins (Fischer and Fowler, 2003). Previously, we showed that rat lens fiber cells contained a short, ∼30-kD TM isoform (Woo and Fowler, 1994). Using a TMCH1 monoclonal antibody that recognizes exon 9a in TMs (Schevzov et al., 2005), an ∼30-kD TM was also detected on blots of whole lens extracts from *Tmod1+/+*$^{Tg+}$ mouse lenses (Fig. 7 A). Western blotting with a TM311 antibody that recognizes exon 1a in long TMs (Schevzov et al., 2005) failed to detect any polypeptides in fiber cells (unpublished data). Biochemical fractionation of cortical fiber cells into cytosol and membranes demonstrated that similar to Tmod1, ∼60–70% of lens TM was associated with membranes in *Tmod1+/+*$^{Tg+}$ lenses (Fig. 7, C and D). To identify this TM, we performed LC/MS-MS on membrane extracts enriched for the ∼30-kD TM, revealing a C-terminal exon 9a peptide from the γTM gene: …K.AISDELDHALNDMTSI-COOH (Lees-Miller and Helfman, 1991). Therefore, the predominant TM in the mouse lens is a short, exon 9a–containing γTM (Gunning et al., 2005; Schevzov et al., 2005).

Western blotting of total cortical fiber cell extracts from age-matched sets of *Tmod1+/+*$^{Tg+}$ and *Tmod1−/−*$^{Tg+}$ mice revealed that total levels of the short γTM in *Tmod1−/−*$^{Tg+}$ lenses were reduced to ∼25% of levels present in *Tmod1+/+*$^{Tg+}$ lenses, whereas total levels of actin were unchanged (Fig. 7, A and B). In addition, most of the residual γTM was in the cytosol in the absence of Tmod1, whereas a majority of the γTM was associated with membranes in the presence of Tmod1 (Fig. 7, C and D). Thus, the membrane-associated portion of the γTM was selectively

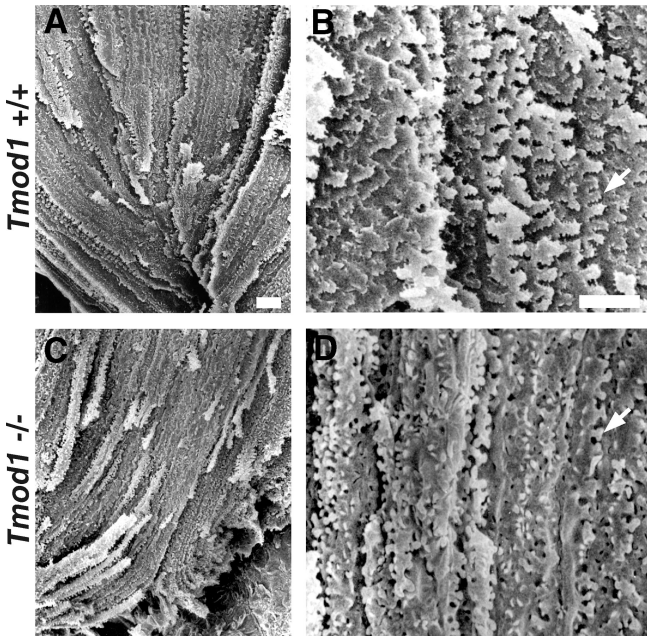

Figure 6. **Membrane protrusions are abnormally shaped and disorganized in fiber cells lacking Tmod1.** Cortical fiber peels from the anterior portion of 5-mo-old *Tmod1+/+$^{Tg+}$* (A and B) and of 8 mo-old *Tmod1−/−$^{Tg+}$* (C and D) mouse lenses, viewed from the inside looking out. Matched regions near the anterior suture depict en face views of the broad sides of overlapping fiber cells. B and D are higher magnification views from similar regions as in A and C. (B and D) Arrows indicate protrusions. Bars, 10 μm.

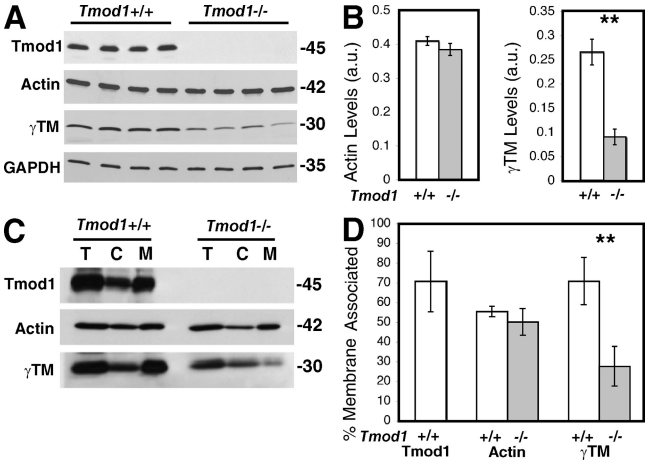

Figure 7. **Mouse lenses lacking Tmod1 have decreased levels of a short γTM, whereas global actin levels are unchanged.** (A) Western blots of Tmod1, actin, γTM, and GAPDH in cortical fiber cell extracts from 2-mo-old mice. Each lane is 1/4 of a lens cortex from a different animal. (B) Quantification from blots in A, normalized to GAPDH. γTM is reduced ~3-fold ($P < 0.002$), but actin is unchanged ($P < 0.96$). $n = 4$ animals per genotype. (C) Western blots of Tmod1, actin, and γTM in total cortical fiber cell extracts (T), cytosol (C), and membranes (M) from 4-mo-old mice. Each lane is 1/10 of a lens cortex. (D) Percentage of membrane-associated Tmod1, actin, or γTM. Percentage of γTM on membranes is ~60% in *Tmod1+/+$^{Tg+}$* and ~30% in *Tmod1−/−$^{Tg+}$* lenses ($P < 0.008$). Actin levels on membranes are unchanged ($P < 0.2$). $n = 3$ experiments.

reduced in the absence of Tmod1, indicating that the γTM does not assemble, or that its association with membranes is unstable in the absence of Tmod1.

Despite the reduction in γTM on the membrane, the overall proportion of membrane-associated actin in lens cortical fiber cells was not significantly altered in the absence of Tmod1 (Fig. 7, C and D). In addition, ultracentrifugation of the cytosol fraction to sediment F-actin oligomers or short polymers showed that all the actin remained in the supernatant both in the presence and absence of Tmod1 (unpublished data). Moreover, Triton X-100 extraction of membranes did not reveal differences in the absence of Tmod1 (see Fig. 9 F). Thus, the absence of Tmod1 and reduction of γTM did not lead to global F-actin depolymerization, suggesting that Tmod1 and γTM may stabilize a subpopulation of F-actin on membranes of cortical fiber cells. This subpopulation of F-actin may be reorganized into a different architecture in the absence of Tmod1, as suggested by decreased F-actin staining and a greater variation in intensity observed in young *Tmod1−/−$^{Tg+}$* lenses (Fig. 4, H and J).

F-actin on fiber cell membranes is disrupted locally in the absence of Tmod1

If Tmod1 selectively stabilizes a subpopulation of membrane-associated γTM–F-actins, we might expect that in the absence of Tmod1, perturbations of membrane F-actin would occur in the membrane domains where Tmod1 normally assembles, i.e., on the broad and narrow sides of fiber cells located ~20–30 cell layers in from the epithelium (Fig. 2 D). To investigate this, we examined F-actin distribution in matched regions of lens sections from *Tmod1+/+$^{Tg+}$* and *Tmod1−/−$^{Tg+}$* mice. In *Tmod1+/+$^{Tg+}$* lenses, F-actin distribution appeared uniform along fiber cell membranes, and was enriched at the vertices of the hexagonally packed fiber cells, as shown in 3D reconstructions of image Z stacks (Fig. 8 A) and in single optical sections (Fig. 8 G). In contrast, F-actin distribution on fiber cell membranes in *Tmod1−/−$^{Tg+}$* lenses had a distinctly irregular and moth-eaten appearance, with many discontinuities or holes, in both hexagonally packed and disordered regions of fiber cells (Fig. 8, B, H, and I). The gaps in F-actin in the absence of Tmod1 were present on both broad and narrow sides, where Tmod1 normally assembles (Fig. 2), as clearly evident at higher magnification when image stacks were tilted and rotated to obtain en face views of broad (Fig. 8 D) or narrow (Fig. 8 F) sides. This contrasts with the smooth and continuous F-actin staining on both the broad and narrow sides in the presence of Tmod1 (Fig. 8, C and E).

To investigate whether irregular F-actin distribution in the absence of Tmod1 is due to F-actin rearrangements or to local F-actin dissociation or depolymerization, we quantified F-actin staining intensity from single optical sections using MetaMorph. Comparison of average F-actin staining intensity in matched fields from *Tmod1+/+$^{Tg+}$* and *Tmod1−/−$^{Tg+}$* lenses showed a significant decrease in mean intensity in the absence of Tmod1 (Fig. 8 J), consistent with F-actin depolymerization in these regions of the lens cortex. However, because this data could be affected by variations in thickness or staining efficiency of sections from different lenses, we also compared the relative percentage of F-actin staining on membranes versus cytoplasm for the images from each genotype. Using the thresholding function in MetaMorph to define areas corresponding to membrane and cytoplasmic F-actin, we determined that

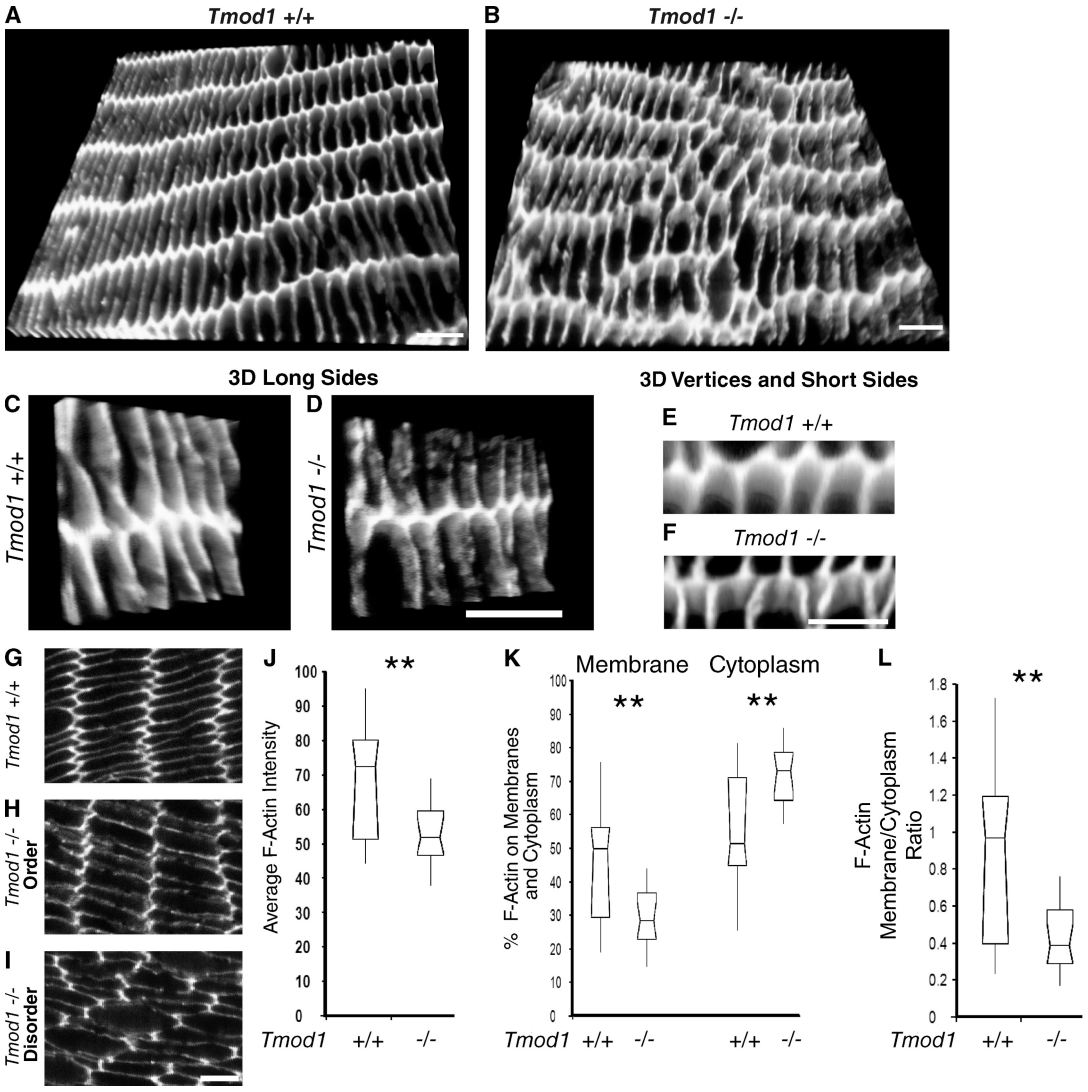

Figure 8. **F-actin is disrupted locally and depleted from fiber cell membranes in the absence of Tmod1.** (A–F) 3D images of Z stacks or (G–I) single optical sections of F-actin showing matched regions of fiber cells ~20–30 cell layers in from the epithelium in equatorial sections of 1-mo-old mouse lenses. 3D images of fiber cells at low (A and B) and high (C–F) magnification, tilted to obtain en face views of broad sides (C and D) or vertices and narrow sides (E and F). Bars: (A and B) 4.6 µm; (C and D) 5 µm; (E–I) 4 µm. (J–L) Quantification of F-actin fluorescence intensities. (J) Average total F-actin, (K) percent F-actin on membranes or cytoplasm, (L) ratio of membrane to cytoplasmic F-actin. n = 22 *Tmod1+/+*$^{Tg+}$ and 20 *Tmod1−/−*$^{Tg+}$ fields of view from three animals per genotype. **, $P < 0.0001$.

F-actin staining was about equally distributed between membranes and cytoplasm in *Tmod1+/+*$^{Tg+}$ lenses (Fig. 8 K). In contrast, only ~30% of the F-actin was associated with membranes in the absence of Tmod1 (Fig. 8 K). Thus, the membrane/cytoplasmic F-actin ratio decreased significantly, by greater than twofold in the absence of Tmod1 (Fig. 8 L). Note that because cytoplasm is defined operationally by the thresh-holding function, a diffuse submembrane cortical region of the fiber cells with weak F-actin staining in the absence of Tmod1 is also included in the cytoplasm (Fig. 8, G and H). These data indicate that absence of Tmod1 led to localized F-actin dissociation or depolymerization from broad and narrow side fiber cell membrane (leading to discontinuities in staining), followed either by translocation of existing filaments or by polymerization of new filaments away from the membrane. These changes in F-actin occurred irrespective of the presence of fiber cell disorder, suggesting that they may precede or underlie the formation of disordered regions of fiber cells in the absence of Tmod1.

The spectrin membrane skeleton in fiber cells is disrupted in the absence of Tmod1

Spectrin and other components of the membrane skeleton are associated with both the broad and narrow sides of fiber cell membranes (Fig. 9) (Nelson et al., 1983; Kaiser et al., 1989; Lee et al., 2000; Moré et al., 2001; Straub et al., 2003). If Tmod1 and γTM stabilize the F-actin linkers in the spectrin–actin network, then the absence of Tmod1 would be expected to lead to disruption and/or disassembly of the spectrin–actin network. To investigate this, we stained lens sections from *Tmod1+/+*$^{Tg+}$ and *Tmod1−/−*$^{Tg+}$ mice with antibodies to β2-spectrin. Examination of high magnification images of single optical sections

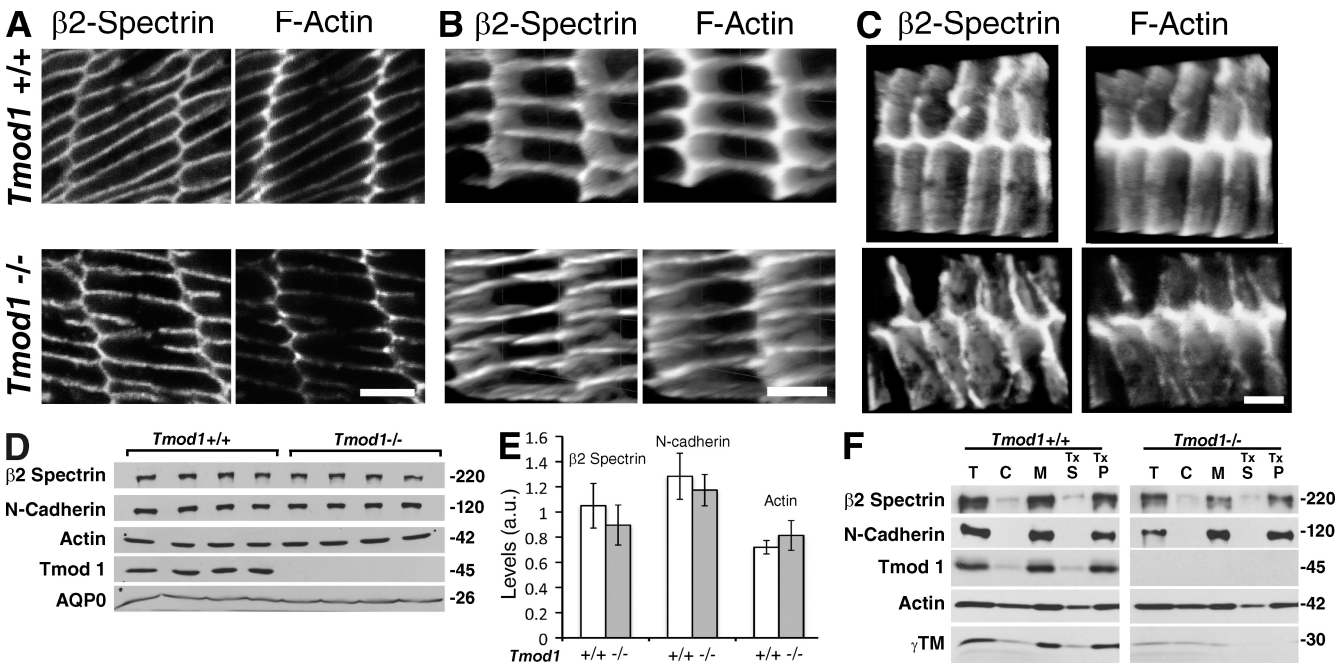

Figure 9. **β2-spectrin organization on fiber cell membranes is disrupted in the absence of Tmod1, but β2-spectrin levels and membrane association are unchanged.** (A) Single optical sections or (B and C) 3D images of Z stacks of β2-spectrin and F-actin showing matched regions of fiber cells from 1-mo-old mouse lenses as in Fig. 8. En face views of vertices and narrow sides (B) or broad sides (C). Bars: (A and B) 4 µm; (C) 2.2 µm. (D) Western blots of β2-spectrin, N-cadherin, actin, Tmod1, and Aquaporin 0 (AQP0) in total cortical fiber cell extracts. Each lane is 1/4 of a 1-mo-old lens cortex from a different animal. (E) Quantification from blots in D, normalized to AQP0. Levels of β2-spectrin, N-cadherin, and actin are not different in absence of Tmod1 ($P < 0.24$, 0.36, and 0.2, respectively). $n = 4$ animals per genotype. (F) Western blots of β2-spectrin, N-cadherin, Tmod1, actin, and γTM in cortical fiber cell total extracts (T), cytosol (C), membranes (M), Triton X-100 supernatant (TxS), and pellet (TxP) from 8-mo-old mice.

from matched regions where Tmod1 normally assembles reveals smooth and continuous β2-spectrin staining along fiber cell membranes in the presence of Tmod1 (Fig. 9 A, top), but somewhat punctate and discontinuous β2-spectrin staining in the absence of Tmod1 (Fig. 9 A, bottom). The increased gaps and irregularities in β2-spectrin staining in the absence but not presence of Tmod1 are more clearly evident in 3D reconstructions from Z stacks, tilted to view the narrow (Fig. 9 B) or broad (Fig. 9 C) sides of the fiber cells. This is strikingly similar to the perturbations in F-actin distribution along membranes in these same fiber cells (Fig. 9, A–C) and as shown above (Fig. 8), and indicates that the absence of Tmod1 leads to disruptions in the spectrin–actin network.

However, Western blotting of cortical fiber cell extracts indicates that global levels of β2-spectrin were not affected significantly by the absence of Tmod1 (Fig. 9, D and E). Total levels of N-cadherin were also unaffected (Fig. 9, D and E). Moreover, the proportions of β2-spectrin, N-cadherin, and actin associated with cortical fiber cell membranes after biochemical fractionation and Triton X-100 extraction were unchanged in the absence of Tmod1 (Fig. 9 F; also see Fig. 7, C and D). Finally, immunofluorescence staining for N-cadherin did not reveal alterations in its staining pattern on fiber cell membranes (unpublished data). Therefore, discontinuities in β2-spectrin distribution on membranes revealed by confocal fluorescence microscopy reflect disruptions in connectivity of the spectrin–actin network due to local F-actin disassembly, rather than reduction in global levels or dissociation of β2-spectrin from membranes in the absence of Tmod1.

Discussion

The hexagonal geometry of lens fiber cells is arguably the most precise example of hexagonal packing for epithelial cells in any tissue or organ known. Here, we show that Tmod1 stabilization of γTM–F-actins in the membrane skeleton is required to maintain membrane morphologies and hexagonal geometries of lens fiber cells. In the absence of Tmod1, disassembly of the γTM–F-actin linkers is accompanied by disruptions in connectivity of the spectrin–actin network and aberrant protrusion morphologies (Fig. 10). The disruption of an elastic spectrin–actin network may perturb balanced tensile forces along fiber cell membranes, leading to membrane instability, altered cell–cell interactions, fiber cell rearrangements, and disordered cell packing. Notably, Tmod1 function is required for the maintenance but not biogenesis of membrane morphologies, fiber cell shapes, and packing geometry. This is analogous to erythrocytes, where defects in the spectrin–actin network result in mechanically unstable membranes that over time in the blood circulation result in cells with irregular contours, protrusions, and blebbing (Mohandas and Evans, 1994; Mohandas and Gallagher, 2008).

A critical function for the membrane skeleton in maintaining cortical fiber cell shapes and organization during maturation is supported by the lens phenotype of mice lacking the membrane skeleton linker protein, ankyrinB, or its transmembrane anchor, NrCAM (Moré et al., 2001). Similar to absence of Tmod1, initial morphogenesis of fiber cells at the bow region of P1 lenses is normal in the absence of either ankyrinB or NrCAM, but abnormal fiber cell shapes and organization, along with perturbations

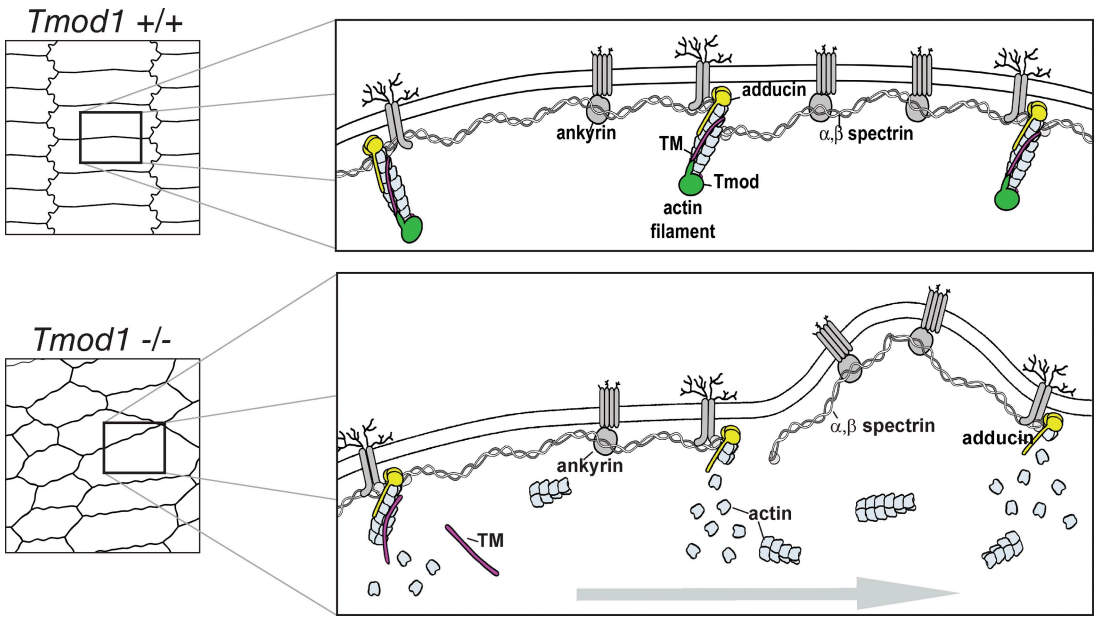

Figure 10. **Molecular mechanism for disruption of the membrane skeleton in the absence of Tmod1.** (Top) Model depicting lens fiber cell hexagonal geometry and molecular organization of the membrane skeleton. The short actin filament linkers in the spectrin–actin network are capped by Tmod1 (green) and adducin (yellow) and stabilized by TM (red). The network is linked to membrane proteins via ankyrin (gray ovals), adducin, and 4.1 adaptor proteins (not depicted) (Bennett and Baines, 2001). (Bottom) Model depicting disordered fiber cell packing in lenses lacking Tmod1, due to a hypothetical progression (horizontal gray arrow) of TM dissociation from actin filaments, followed by depolymerization of the short actin filament linkers and disruption of spectrin network connections, leading to membrane instability and abnormal protrusions.

in F-actin distribution, appear in maturing fiber cells in the cortex, especially near the anterior of the lens. The phenotype of ankyrinB or NrCAM null lenses is considerably more severe than that of Tmod1 null lenses, likely because complete loss of membrane attachment of the spectrin–actin network is more deleterious. Indeed, the absence of Tmod1 does not affect total levels of β2-spectrin or its association with membranes, consistent with β2-spectrin linking to membranes via binding sites such as ankyrinB and integral membrane proteins that do not depend on F-actin (Bennett and Baines, 2001).

Previous studies on actin function in the lens have shown that regulation of F-actin assembly is important for lens epithelial to fiber cell differentiation and for fiber cell elongation and migration (Fischer et al., 2000; Grove et al., 2004; Zelenka, 2004; Rao and Maddala, 2006; Weber and Menko, 2006; Chen et al., 2008; Maddala et al., 2008). In contrast, absence of Tmod1 does not affect fiber cell initial differentiation and morphogenesis. Instead, Tmod1 stabilizes γTM–F-actins in the membrane skeleton during cortical fiber cell maturation before organelle loss. Furthermore, Tmod1 appears to selectively stabilize a subset of F-actins in the membrane skeleton, while leaving other F-actins unaffected, as indicated by the partial decrease in F-actin from membranes in the absence of Tmod1. In particular, the absence of Tmod1 does not appear to affect the α-actinin–cross-linked F-actin bundles that run along the lengths of fiber cells near their vertices (Lo et al., 1997), based on the persistence of bright F-actin staining at vertices in the absence of Tmod1.

In addition to F-actins, lens fiber cells contain a specialized type of intermediate filament, the beaded filament, comprised of two obligate assembly partners, CP49 and filensin. Lenses without beaded filaments exhibit normal fiber cell differentiation and elongation, as well as normal fiber cell morphology throughout their maturation in the cortex (Alizadeh et al., 2002, 2003; Yoon et al., 2008). However, although the interlocking paddle-like membrane protrusions appear to form normally in cortical fiber cells, they do not persist upon organelle and nuclear loss and the nuclear fiber cells instead exhibit smooth membrane contours with no protrusions (Sandilands et al., 2003; Yoon et al., 2008). This phenotype differs from lenses without Tmod1, where fiber cell protrusions are present but abnormally shaped and mislocalized on the cortical fiber cells. Nevertheless, because our studies of *Tmod1*$-/-^{Tg+}$ mice were performed in a strain background with a spontaneous mutation in the *Bfsp2/CP49* gene, resulting in absence of CP49 protein and reduced levels of filensin (Fig. S3) (Alizadeh et al., 2004; Sandilands et al., 2004; Simirskii et al., 2006), it is possible that lack of beaded filaments could contribute to the effects of Tmod1 deletion on fiber cell morphology.

Tmod1 regulates actin polymerization and stability via TM

The molecular phenotype of lenses lacking Tmod1 is similar to siRNA knockdown of Tmod3 in polarized Caco2 intestinal epithelial cells, which results in selective reductions of TM and F-actin from lateral membranes along with disrupted spectrin organization (Weber et al., 2007). Decreased F-actin on membranes in the absence of Tmod1 may result from enhanced accessibility of TM-free F-actins to ADF/cofilin or gelsolin-mediated severing and disassembly (Cooper, 2002; Gunning et al., 2005). F-actins without TM are also better substrates for Arp2/3-stimulated polymerization of dendritic actin networks,

such as in lamellipodia (Cooper, 2002; Gunning et al., 2005). Thus, TM-free F-actins in the absence of Tmod1 may be redistributed by severing and depolymerization followed by nucleation and reassembly in ectopic locations, accounting for the observed shift of F-actin from membranes to the cytoplasm in absence of Tmod1 (Fig. 8). Such aberrant polymerization of F-actin in the absence of Tmod was also observed for siRNA knockdown of Tmod3 in migrating human microvascular endothelial cells (Fischer et al., 2003), where more F-actin was generated in the leading lamellipodia via enhanced Arp2/3-induced nucleation from TM-free F-actins. Future analysis of the "actin economy" (Pollard et al., 2000) in lens fiber cells may shed light on how regulation of actin polymerization contributes to stability of the spectrin–actin membrane skeleton and maintenance of fiber cell shapes and membrane morphologies.

Role of membrane skeleton network connectivity in hexagonal packing geometry

While not recognized at the time, a role for spectrin network connectivity in epithelial cell packing geometry was revealed over 10 years ago by the disorganized cellular packing observed in the *Drosophila* follicular cell epithelium for α-spectrin mutants defective in dimer–tetramer formation, which were unable to form a long-range spectrin–actin network (Deng et al., 1995). Our conclusions are also supported by recent studies on α-adducin (Abdi and Bennett, 2008), a membrane skeleton protein that promotes spectrin–actin complex formation and caps barbed filament ends (Kuhlman et al., 1996; Li et al., 1998). Similar to effects of Tmod3 knockdown in Caco2 epithelial cells (Weber et al., 2007), shRNA knockdown of α-adducin in cultured human bronchiole epithelial (HBE) cells leads to shorter and wider cells without disturbing apical–basal cell polarity (Abdi and Bennett, 2008). In the absence of α-adducin, β2-spectrin and ankyrinG association with the membrane skeleton is reduced and E-cadherin diffusion in the plasma membrane is unrestricted, indicative of disruptions in long-range network connectivity. Strikingly, α-adducin–depleted cells exhibited excessive lateral membrane curvature and aberrant pentagonal shapes when surrounded by normal cells, in contrast to the hexagonal geometry characteristic of wild-type cells. Similar to Tmod1 in lens fiber cells, α-adducin was not required for the biogenesis of cell shapes, but rather for their maintenance in mature polarized HBE monolayers.

Previous work has shown that forces determining cell shapes and packing geometry are determined by the strength of cadherin-mediated cell adhesion, and by actomyosin contraction along lateral membranes (Carthew, 2005; Farhadifar et al., 2007; Lecuit and Lenne, 2007; Martin et al., 2009). Our study here on Tmod1 in lens fiber cells, and that of the Bennett laboratory on α-adducin in HBE cells (Abdi and Bennett, 2008) both suggest that the long-range connectivity of an intrinsically elastic spectrin–actin network (Mohandas and Evans, 1994) also contributes to the balanced distribution of forces along membranes that control hexagonal geometry. A uniformly distributed, elastic spectrin–actin network could influence distributions of cell–cell adhesion molecules along lateral membranes, promoting balanced intercellular adhesive forces required for hexagonal packing of adjacent cells. Alternatively, an elastic spectrin–actin network might serve to distribute actomyosin contractile forces evenly along lateral membranes, particularly if myosin were to interact directly with the F-actins of the spectrin–actin network (Fowler, 1986).

A surprising finding in our study was the sporadic appearance of abnormal fiber cell shapes and disordered packing despite the disruption of the spectrin–actin network in all cortical fiber cells of Tmod1 null lenses. This may reflect the fact that fiber cells in the same layer (i.e., of the same age) are not all morphologically equivalent in the mouse lens (Kuszak et al., 2004a,b, 2006). Namely, although fiber cells contacting the ends of the Y-shaped suture branches of the mouse lens are aligned with respect to the optic axis, the fiber cells contacting the middles of the suture branches exhibit S-shaped curvatures with respect to the optic axis (Fig. 1 C; Fig. S1). Thus, sporadic perturbations in cell packing we observe in the absence of Tmod1 with disrupted spectrin–actin network organization may reflect varying responses of the differently shaped fiber cells to external or internal forces acting on the lens. The complex 3D fiber cell shapes and their hexagonal packing geometry stabilized by an elastic spectrin–actin network may be important to resist forces that arise during lens growth, accommodation, or eye movements, as well as to minimize light scattering for optical quality and focusing (Tardieu, 1988).

Materials and methods

Mice and genotyping

A viable *Tmod1* null mouse line was generated by crossing *Tmod1*$^{lacZ+/-}$ mice (Fritz-Six et al., 2003) with mice expressing a *Tmod1* transgene only in the heart (*Tg(αMHC-Tmod1)*, and maintained as heterozygotes (*Tmod1+/−*$^{Tg(\alpha MHC\text{-}Tmod1)}$) (McKeown et al., 2008). The *Tg(αMHC-Tmod1)* mice were generated on the FVB/N background (Sussman et al., 1998), which has an endogenous mutation in the *Bfsp2/CP49* gene (Simirskii et al., 2006). Thus, lenses from our strain of *Tmod1+/−*$^{Tg(\alpha MHC\text{-}Tmod1)}$ mice are missing the beaded filament protein, CP49, and have reduced levels of filensin (Fig. S3). Phenotypic analyses of 2-mo-old mice or older were performed on progeny derived from crosses of *Tmod1+/−* mice with *Tmod1+/−*$^{Tg(\alpha MHC\text{-}Tmod1)}$ mice (∼1/8 of progeny are null for endogenous *Tmod1*). Analyses on lenses from 1-mo-old or younger animals were performed on progeny generated by intercrosses of either *Tmod1+/+*$^{Tg(\alpha MHC\text{-}Tmod1)}$ or *Tmod1−/−*$^{Tg(\alpha MHC\text{-}Tmod1)}$ mice (in this case, all progeny in a litter were *Tg+* and either *Tmod1+/+* or *Tmod1−/−*). Genotyping was performed by PCR as described previously (McKeown et al., 2008). All procedures were in accordance with The Scripps Research Institute animal care guidelines.

Lens morphology and light and electron microscopy

Lenses from eyes of age-matched animals were dissected in Dulbecco's PBS (DPBS) at 37°C and photographed using oblique illumination on a dissecting microscope (model SZ11; Olympus) with a camera (CoolPix990; Nikon). Lens equatorial diameters were measured by including a ruler in the images. Lens weights were measured after blotting lenses dry with a Kim-Wipe (Kimberly-Clark). For light microscopy of sections of adult lenses (Fig. 5), lenses were dissected, fixed in 2.5% glutaraldehyde, embedded in epoxy resin, and 1-µm sagittal sections were cut through the lens parallel to the optic axis (Chung et al., 2007). Sections were stained with methylene blue and azure II and micrographs acquired with a microscope (Vanox AHBS3; Olympus) with a 35-mm camera. Fiber cell organization at the anterior and posterior of the lens was measured by tracing paths from one cell to the next adjacent cell along the radial columns, and counting the numbers of branch points. Results are means ± SD. For SEM, lenses were prepared as described previously (Chung et al., 2007) and en face views of cortical fiber cells from matching regions of lenses were examined on a scanning electron microscope (JSM 35 cSEM; JEOL USA) at 15 kV; photomicrographs were obtained with a Polaroid camera system (Chung et al., 2007).

Fluorescence staining

For immunofluorescence staining, eyes from P13 to 1-mo-old animals were dissected in PBS, cut open at the posterior pole, fixed in 1% paraformaldehyde in PBS for 4 h at 4°C, followed by incubation overnight in 30% sucrose in PBS and embedding in OCT. Blocks were stored at −80°C until cryosectioning at 12–15 µm on a Cryostat (Cryocut 1800; Leica). Sagittal or equatorial sections were dried on slides and stored up to 10 d at −20°C. Sections were rehydrated in PBST (PBS + 0.1% Triton X-100) for 15 min, permeabilized in PBS + 0.3% Triton X-100 for 15–30 min, and blocked with 4% BSA/1% goat serum in PBST for 1–2 h. For each experiment, sequential sections (one every 50–100 µm) from each lens were labeled with primary antibody in blocking buffer overnight at 4°C, washed 3 × 20 min in PBST, then labeled for 1.5–2 h with a fluorescent-conjugated secondary antibody mixture containing fluorescent phalloidin to label F-actin and Hoechst dye to stain nuclei. After washing 3 × 20 min in PBST, sections were cover slipped using Gel/Mount (BioMedia). All steps were at room temperature unless otherwise indicated. Rhodamine- or Alexa Fluor 568–labeled phalloidin (1:200 of 200 units/ml; Invitrogen) was used to label F-actin, and Hoechst 332 dye (100 ng/µl; Sigma-Aldrich) to label nuclei. Primary antibodies used were rabbit polyclonal antibody against human Tmod1 (R1749) (2 µg/ml) and mouse monoclonals against TM (TMCH1) (15 µg/ml; Developmental Studies Hybridoma Bank, Iowa City, IA), and β2-spectrin (42/B) (0.5 µg/ml; BD Biosciences). Secondary antibodies were Alexa Fluor 488 goat anti–rabbit or Alexa Fluor 647 goat anti–mouse (Invitrogen).

Imaging and quantitative analyses

Images were acquired at room temperature using a laser-scan confocal microscope (Radiance 2100; Bio-Rad Laboratories) mounted on a Nikon microscope using the following objective lenses: 10X/0.45 NA (Fig. 2, A–C; Fig. S2), 20X/0.75 NA (Fig. 4, G and H), 100X/1.4 NA oil, zoom 1 (Fig. 2, D–F; Fig. 4, A–D; Fig. 8, A and B) or zoom 2.6 (Fig. 2, G–S; Fig. 4, E and F; Fig. 8, C–I; Fig. 9). For Z stacks with the 100X lens (Figs. 8 and 9), the step size was in the range of 0.3 µm, and 10 optical sections, ∼1-µm thick, were collected. Images were processed using Volocity 5.0.3 and Adobe Photoshop and image figures constructed in Adobe Illustrator. Images presented of *Tmod1+/+$^{Tg+}$* and *Tmod1−/−$^{Tg+}$* lenses are from matched sections obtained from the same position and orientation in the lens, as determined by epithelium thickness, positions of fiber cell nuclei, and morphology of fiber cells. Quantifications of fluorescence intensity were performed with MetaMorph (MDS Analytical Technologies), statistical analyses with Microsoft Excel, and box-and-whisker plots with Analyze-It (Analyze-It Software). To determine fiber cell organization in Fig. 4, G–K, linescans of F-actin intensity, 11.6 µm wide (20 pixels) and ∼250–300 µm long, were performed in MetaMorph on images acquired at 20X (zoom 1). Variability in intensity was determined from 10 line scans averaged from 2 sections each of *Tmod1+/+$^{Tg+}$* and *Tmod1−/−$^{Tg+}$* P13 lenses, calculated by measuring the variation in the standard deviation of the fluorescence intensity along the linescan. Results are means ± SD. To determine average total F-actin intensities in Fig. 8 J, single optical section images of the bow region, containing 5–6 columns of fiber cell profiles, were acquired using the 100X lens at zoom 2.6 and pixel intensities of matched fields determined in MetaMorph. To determine relative membrane and cytoplasmic F-actin (Fig. 8, K and L), pixel intensities in one field from a *Tmod1+/+$^{Tg+}$* lens section were subdivided into two intensity categories (membranes or cytoplasm) using the thresh-holding function in MetaMorph. The intensity thresh-holding values from this field were assigned to all other images from both *Tmod1+/+$^{Tg+}$* and *Tmod1−/−$^{Tg+}$* sections, then intensities of membranes and cytoplasm determined for each set of images from the two genotypes, and results presented as box-and-whisker plots. 22 *Tmod1+/+$^{Tg+}$* and 20 *Tmod1−/−$^{Tg+}$* fields of view from 3 animals of each genotype (3 experiments) were analyzed for Fig. 8, J–L.

Preparation of lens extracts and Western blotting

Lenses were dissected in warmed Ca-Mg–free DPBS, decapsulated, and immediately placed in ice-cold lens buffer (LB) (100 µl for two lenses from one mouse) containing 100 mM KCl, 5 mM EDTA, 10 mM sodium phosphate, pH 7.4, 2 mM dithiothreitol, 5 µg/ml leupeptin/pepstatin, 1:1,000 Aprotinin, and a 1:1,000 dilution of a protease inhibitor cocktail (Sigma-Aldrich). For Figs. 7 and 9, the homogenization buffer also contained sodium fluoride, sodium orthovanadate, and sodium pyrophosphate as described previously (Maddala et al., 2007). Cortical fiber cells were separated from the hard lens nucleus by vortexing for 3–5 times for 10 s at setting #10 on a Vortex mixer, cooling on ice between each vortexing. Fiber cells were sonicated with a microprobe on ice, and total extracts for SDS-PAGE prepared by addition of an equal volume of 5X Laemmli sample buffer and heating for 15–20 min at 42°C. The SDS-solubilized proteins were transferred to a new tube, leaving the hard nucleus behind. To prepare lens cytosol and membrane fractions from cortical fiber cells, decapsulated lenses were pooled from 4 mice (8 lenses) and added to 200 µl LB in a weighed microfuge tube and disrupted by vortexing as above, followed by removal of the hard lens nucleus using a needle. After addition of more LB to bring the final volume to 4–6X of total lens wet weights, cortical fiber cells were homogenized in a 2-ml Dounce glass homogenizer with a teflon pestle (10 strokes) on ice, a portion removed for the "Total" sample, followed by centrifugation for 20 min at 25,000 *g* in a rotor (TLA100.3; Beckman Coulter) at 4°C. The cytosol was taken off, the membrane pellet was resuspended to the initial volume in LB, and samples were solubilized for SDS-PAGE as above. In some experiments, membranes were further extracted by incubation for 60 min with ice-cold 2% Triton X-100 in LB followed by centrifugation and preparation of gel samples as above. To identify lens TM, TMs were enriched by extracting lens membranes in 1 M NaCl in LB, followed by SDS-PAGE and Coomassie staining. The ∼30 kD region of the gel containing TM (determined by Western blotting of a duplicate gel) was excised, followed by proteolytic digestion and LC/MS-MS to identify TM peptides, performed in the TSRI Mass Spectrometry Facility.

Proteins were separated on 7.5–15% linear gradient SDS-polyacrylamide gels and transferred to nitrocellulose for Western blotting in transfer buffer with 20% methanol at 4–15°C as described previously (Fowler, 1990). For β2-spectrin and N-cadherin, the gels were cut in half near the 75-kD marker, and the top halves were transferred without methanol in 0.01% SDS for 3 h at 4°C. The bottom halves were transferred in methanol as usual and blotted for Tmod1, actin, TM, and GAPDH or AQP0 for normalization. Between 1/10 and 1/4 of a lens equivalent was loaded for each sample. Antibodies used were rabbit polyclonal antibodies to human Tmod1 (R1749) at 1 µg/ml (Fowler, 1990; Fritz-Six et al., 2003) and to AQP0 (MP26) at 2 µg/ml (Millipore). Mouse monoclonal antibodies used were C4 to actin at 10 ng/ml (a gift from Dr. J. Lessard, University of Cincinnati, Cincinnati, OH), GAPDH at 1:10,000 (Novus), TMCH1 to TM exon 9a at 1.5 µg/ml (Developmental Studies Hybridoma Bank), 42/B to β2-spectrin at 50 ng/ml (BD Biosciences), and 3B9 to N-cadherin at 0.5 µg/ml (3B9) (Invitrogen). Anti–mouse HRP (Promega) or anti–protein-A-HRP (Sigma-Aldrich) were used for secondary detection, visualized by ECL. Bands on blots were quantified using ImageJ and statistical analyses performed using Microsoft Excel. Results are means ± SD. For quantification of percentage of Tmod1, TM, and actin associated with membranes, the percentage on membranes is calculated as percentage of cytosol + membranes.

Online supplemental material

Figure S1 is a 3D-CAD (computer-assisted drawing) stereo pair diagram of fiber cells in the mouse lens illustrating the different types of fiber cell curvature with respect to the optic axis. Figure S2 shows confocal fluorescence images of sagittal cryosections from *Tmod1+/+$^{Tg+}$* and *Tmod1−/−$^{Tg+}$* mouse lenses stained for Tmod1, F-actin, and nuclei, and demonstrates that initial fiber cell morphogenesis is normal in the absence of Tmod1. Figure S3 shows Western blots and Coomassie blue–stained gels of lens cortical fiber cells from our *Tmod1+/+$^{Tg+}$* and *Tmod1−/−$^{Tg+}$* mice, demonstrating that this strain background is missing the CP49 beaded filament protein in the lens (Simirskii et al., 2006). Figure S4 shows confocal fluorescence images of equatorial cryosections of fiber cells ∼50 cell layers in from the epithelium, revealing that Tmod1 is present in the regions where the paddle-like membrane protrusions are located. Online supplemental material is available at http://www.jcb.org/cgi/content/full/jcb.200905065/DC1.

We thank Jeannette Moyer for help with Western blots, Layne Novak for fixing and sectioning of adult lenses, Renee Chow for black and white line drawings, Mike Mazurkiewicz for 3D-CAD schematic, and members of the Fowler laboratory for discussions and editorial suggestions. We are grateful to Paul Fitzgerald for antibodies to CP49 and filensin and for sharing his results on *CP49−/−* lenses with us before publication. We thank Vann Bennett for polyclonal antibodies to spectrin and ankyrin, and Fritz Rathjen for antibodies to NrCAM.

This work was supported by National Institutes of Health grants to V.M. Fowler (EY017724), R.S. Fischer (EY014972), and J.R. Kuszak (EY06642); and by a National Eye Institute Core Grant for Vision Research (P30-EY12598). This is TSRI manuscript no. 20165.

Submitted: 13 May 2009
Accepted: 14 August 2009

References

Abdi, K.M., and V. Bennett. 2008. Adducin promotes micrometer-scale organization of beta2-spectrin in lateral membranes of bronchial epithelial cells. *Mol. Biol. Cell.* 19:536–545. doi:10.1091/mbc.E07-08-0818

Alizadeh, A., J.I. Clark, T. Seeberger, J. Hess, T. Blankenship, A. Spicer, and P.G. FitzGerald. 2002. Targeted genomic deletion of the lens-specific intermediate filament protein CP49. *Invest. Ophthalmol. Vis. Sci.* 43:3722–3727.

Alizadeh, A., J. Clark, T. Seeberger, J. Hess, T. Blankenship, and P.G. FitzGerald. 2003. Targeted deletion of the lens fiber cell-specific intermediate filament protein filensin. *Invest. Ophthalmol. Vis. Sci.* 44:5252–5258. doi:10.1167/iovs.03-0224

Alizadeh, A., J. Clark, T. Seeberger, J. Hess, T. Blankenship, and P.G. FitzGerald. 2004. Characterization of a mutation in the lens-specific CP49 in the 129 strain of mouse. *Invest. Ophthalmol. Vis. Sci.* 45:884–891. doi:10.1167/iovs.03-0677

Allen, D.P., P.S. Low, A. Dola, and H. Maisel. 1987. Band 3 and ankyrin homologues are present in eye lens: evidence for all major erythrocyte membrane components in same non-erythroid cell. *Biochem. Biophys. Res. Commun.* 149:266–275. doi:10.1016/0006-291X(87)91634-2

Bassnett, S. 2009. On the mechanism of organelle degradation in the vertebrate lens. *Exp. Eye Res.* 88:133–139. doi:10.1016/j.exer.2008.08.017

Bassnett, S., and P.A. Winzenburger. 2003. Morphometric analysis of fibre cell growth in the developing chicken lens. *Exp. Eye Res.* 76:291–302. doi:10.1016/S0014-4835(02)00315-9

Bennett, V., and A.J. Baines. 2001. Spectrin and ankyrin-based pathways: metazoan inventions for integrating cells into tissues. *Physiol. Rev.* 81: 1353–1392.

Bennett, V., and J. Healy. 2008. Organizing the fluid membrane bilayer: diseases linked to spectrin and ankyrin. *Trends Mol. Med.* 14:28–36. doi:10.1016/j.molmed.2007.11.005

Blankenship, T., L. Bradshaw, B. Shibata, and P. Fitzgerald. 2007. Structural specializations emerging late in mouse lens fiber cell differentiation. *Invest. Ophthalmol. Vis. Sci.* 48:3269–3276. doi:10.1167/iovs.07-0109

Byers, T.J., and D. Branton. 1985. Visualization of the protein associations in the erythrocyte membrane skeleton. *Proc. Natl. Acad. Sci. USA.* 82:6153–6157. doi:10.1073/pnas.82.18.6153

Carthew, R.W. 2005. Adhesion proteins and the control of cell shape. *Curr. Opin. Genet. Dev.* 15:358–363. doi:10.1016/j.gde.2005.06.002

Cavey, M., M. Rauzi, P.F. Lenne, and T. Lecuit. 2008. A two-tiered mechanism for stabilization and immobilization of E-cadherin. *Nature.* 453:751–756. doi:10.1038/nature06953

Chen, Y., R.J. Stump, F.J. Lovicu, A. Shimono, and J.W. McAvoy. 2008. Wnt signaling is required for organization of the lens fiber cell cytoskeleton and development of lens three-dimensional architecture. *Dev. Biol.* 324:161–176. doi:10.1016/j.ydbio.2008.09.002

Chu, X., J. Chen, M.C. Reedy, C. Vera, K.L. Sung, and L.A. Sung. 2003. E-Tmod capping of actin filaments at the slow-growing end is required to establish mouse embryonic circulation. *Am. J. Physiol. Heart Circ. Physiol.* 284:H1827–H1838.

Chung, J., V.M. Berthoud, L. Novak, R. Zoltoski, B. Heilbrunn, P.J. Minogue, X. Liu, L. Ebihara, J. Kuszak, and E.C. Beyer. 2007. Transgenic overexpression of connexin50 induces cataracts. *Exp. Eye Res.* 84:513–528. doi:10.1016/j.exer.2006.11.004

Cooper, J.A. 2002. Actin dynamics: tropomyosin provides stability. *Curr. Biol.* 12:R523–R525. doi:10.1016/S0960-9822(02)01028-X

Deng, H., J.K. Lee, L.S. Goldstein, and D. Branton. 1995. *Drosophila* development requires spectrin network formation. *J. Cell Biol.* 128:71–79. doi:10.1083/jcb.128.1.71

Dubreuil, R.R. 2006. Functional links between membrane transport and the spectrin cytoskeleton. *J. Membr. Biol.* 211:151–161. doi:10.1007/s00232-006-0863-y

Faquin, W.C., A. Husain, J. Hung, and D. Branton. 1988. An immunoreactive form of erythrocyte protein 4.9 is present in non-erythroid cells. *Eur. J. Cell Biol.* 46:168–175.

Farhadifar, R., J.C. Röper, B. Aigouy, S. Eaton, and F. Jülicher. 2007. The influence of cell mechanics, cell-cell interactions, and proliferation on epithelial packing. *Curr. Biol.* 17:2095–2104. doi:10.1016/j.cub.2007.11.049

Fischer, R.S., and V.M. Fowler. 2003. Tropomodulins: life at the slow end. *Trends Cell Biol.* 13:593–601. doi:10.1016/j.tcb.2003.09.007

Fischer, R.S., A. Lee, and V.M. Fowler. 2000. Tropomodulin and tropomyosin mediate lens cell actin cytoskeleton reorganization in vitro. *Invest. Ophthalmol. Vis. Sci.* 41:166–174.

Fischer, R.S., K.L. Fritz-Six, and V.M. Fowler. 2003. Pointed-end capping by tropomodulin3 negatively regulates endothelial cell motility. *J. Cell Biol.* 161:371–380. doi:10.1083/jcb.200209057

Fowler, V.M. 1986. An actomyosin contractile mechanism for erythrocyte shape transformations. *J. Cell. Biochem.* 31:1–9. doi:10.1002/jcb.240310102

Fowler, V.M. 1987. Identification and purification of a novel Mr 43,000 tropomyosin-binding protein from human erythrocyte membranes. *J. Biol. Chem.* 262:12792–12800.

Fowler, V.M. 1990. Tropomodulin: a cytoskeletal protein that binds to the end of erythrocyte tropomyosin and inhibits tropomyosin binding to actin. *J. Cell Biol.* 111:471–481. doi:10.1083/jcb.111.2.471

Fowler, V.M. 1996. Regulation of actin filament length in erythrocytes and striated muscle. *Curr. Opin. Cell Biol.* 8:86–96. doi:10.1016/S0955-0674(96)80052-4

Fritz-Six, K.L., P.R. Cox, R.S. Fischer, B. Xu, C.C. Gregorio, H.Y. Zoghbi, and V.M. Fowler. 2003. Aberrant myofibril assembly in tropomodulin1 null mice leads to aborted heart development and embryonic lethality. *J. Cell Biol.* 163:1033–1044. doi:10.1083/jcb.200308164

Gibson, M.C., A.B. Patel, R. Nagpal, and N. Perrimon. 2006. The emergence of geometric order in proliferating metazoan epithelia. *Nature.* 442:1038–1041. doi:10.1038/nature05014

Gilligan, D.M., and V. Bennett. 1993. The junctional complex of the membrane skeleton. *Semin. Hematol.* 30:74–83.

Green, J.B., and L.A. Davidson. 2007. Convergent extension and the hexahedral cell. *Nat. Cell Biol.* 9:1010–1015. doi:10.1038/ncb438

Grove, M., G. Demyanenko, A. Echarri, P.A. Zipfel, M.E. Quiroz, R.M. Rodriguiz, M. Playford, S.A. Martensen, M.R. Robinson, W.C. Wetsel, et al. 2004. ABI2-deficient mice exhibit defective cell migration, aberrant dendritic spine morphogenesis, and deficits in learning and memory. *Mol. Cell. Biol.* 24:10905–10922. doi:10.1128/MCB.24.24.10905-10922.2004

Gunning, P.W., G. Schevzov, A.J. Kee, and E.C. Hardeman. 2005. Tropomyosin isoforms: divining rods for actin cytoskeleton function. *Trends Cell Biol.* 15:333–341. doi:10.1016/j.tcb.2005.04.007

Gustafsson, M.G. 1999. Extended resolution fluorescence microscopy. *Curr. Opin. Struct. Biol.* 9:627–634. doi:10.1016/S0959-440X(99)00016-0

Jones, C., and P. Chen. 2007. Planar cell polarity signaling in vertebrates. *Bioessays.* 29:120–132. doi:10.1002/bies.20526

Käfer, J., T. Hayashi, A.F. Marée, R.W. Carthew, and F. Graner. 2007. Cell adhesion and cortex contractility determine cell patterning in the *Drosophila* retina. *Proc. Natl. Acad. Sci. USA.* 104:18549–18554. doi:10.1073/pnas.0704235104

Kaiser, H.W., E. O'Keefe, and V. Bennett. 1989. Adducin: Ca++-dependent association with sites of cell-cell contact. *J. Cell Biol.* 109:557–569. doi:10.1083/jcb.109.2.557

Kizhatil, K., and V. Bennett. 2004. Lateral membrane biogenesis in human bronchial epithelial cells requires 190-kDa ankyrin-G. *J. Biol. Chem.* 279:16706–16714. doi:10.1074/jbc.M314296200

Kizhatil, K., J.Q. Davis, L. Davis, J. Hoffman, B.L. Hogan, and V. Bennett. 2007a. Ankyrin-G is a molecular partner of E-cadherin in epithelial cells and early embryos. *J. Biol. Chem.* 282:26552–26561. doi:10.1074/jbc.M703158200

Kizhatil, K., W. Yoon, P.J. Mohler, L.H. Davis, J.A. Hoffman, and V. Bennett. 2007b. Ankyrin-G and beta2-spectrin collaborate in biogenesis of lateral membrane of human bronchial epithelial cells. *J. Biol. Chem.* 282:2029–2037. doi:10.1074/jbc.M608921200

Kuhlman, P.A., C.A. Hughes, V. Bennett, and V.M. Fowler. 1996. A new function for adducin. Calcium/calmodulin-regulated capping of the barbed ends of actin filaments. *J. Biol. Chem.* 271:7986–7991. doi:10.1074/jbc.271.14.7986

Kuszak, J.R., K.L. Peterson, and H.G. Brown. 1996. Electron microscopic observations of the crystalline lens. *Microsc. Res. Tech.* 33:441–479. doi:10.1002/(SICI)1097-0029(19960415)33:6<441::AID-JEMT1>3.0.CO;2-O

Kuszak, J.R., R.K. Zoltoski, and C. Sivertson. 2004a. Fibre cell organization in crystalline lenses. *Exp. Eye Res.* 78:673–687. doi:10.1016/j.exer.2003.09.016

Kuszak, J.R., R.K. Zoltoski, and C.E. Tiedemann. 2004b. Development of lens sutures. *Int. J. Dev. Biol.* 48:889–902. doi:10.1387/ijdb.041880jk

Kuszak, J.R., M. Mazurkiewicz, and R. Zoltoski. 2006. Computer modeling of secondary fiber development and growth: I. Nonprimate lenses. *Mol. Vis.* 12:251–270.

Lecuit, T., and P.F. Lenne. 2007. Cell surface mechanics and the control of cell shape, tissue patterns and morphogenesis. *Nat. Rev. Mol. Cell Biol.* 8:633–644. doi:10.1038/nrm2222

Lee, A., R.S. Fischer, and V.M. Fowler. 2000. Stabilization and remodeling of the membrane skeleton during lens fiber cell differentiation and maturation. *Dev. Dyn.* 217:257–270. doi:10.1002/(SICI)1097-0177(200003)217:3<257::AID-DVDY4>3.0.CO;2-5

Lee, A., J.S. Morrow, and V.M. Fowler. 2001. Caspase remodeling of the spectrin membrane skeleton during lens development and aging. *J. Biol. Chem.* 276:20735–20742. doi:10.1074/jbc.M009723200

Lees-Miller, J.P., and D.M. Helfman. 1991. The molecular basis for tropomyosin isoform diversity. *Bioessays.* 13:429–437. doi:10.1002/bies.950130902

Li, X., Y. Matsuoka, and V. Bennett. 1998. Adducin preferentially recruits spectrin to the fast growing ends of actin filaments in a complex requiring the MARCKS-related domain and a newly defined oligomerization domain. *J. Biol. Chem.* 273:19329–19338. doi:10.1074/jbc.273.30.19329

Liu, S.C., L.H. Derick, and J. Palek. 1987. Visualization of the hexagonal lattice in the erythrocyte membrane skeleton. *J. Cell Biol.* 104:527–536. doi:10.1083/jcb.104.3.527

Lo, W.K., A.P. Shaw, and X.J. Wen. 1997. Actin filament bundles in cortical fiber cells of the rat lens. *Exp. Eye Res.* 65:691–701. doi:10.1006/exer.1997.0375

Luna, E.J., and A.L. Hitt. 1992. Cytoskeleton–plasma membrane interactions. *Science.* 258:955–964. doi:10.1126/science.1439807

Maddala, R., N. Skiba, and P. Vasantha Rao. 2007. Lens fiber cell elongation and differentiation is associated with a robust increase in myosin light chain phosphorylation in the developing mouse. *Differentiation.* 75:713–725. doi:10.1111/j.1432-0436.2007.00173.x

Maddala, R., L.W. Reneker, B. Pendurthi, and P.V. Rao. 2008. Rho GDP dissociation inhibitor-mediated disruption of Rho GTPase activity impairs lens fiber cell migration, elongation and survival. *Dev. Biol.* 315:217–231. doi:10.1016/j.ydbio.2007.12.039

Martin, A.C., M. Kaschube, and E.F. Wieschaus. 2009. Pulsed contractions of an actin-myosin network drive apical constriction. *Nature.* 457:495–499. doi:10.1038/nature07522

McAvoy, J.W., C.G. Chamberlain, R.U. de Iongh, A.M. Hales, and F.J. Lovicu. 1999. Lens development. *Eye.* 13:425–437.

McKeown, C.R., R.B. Nowak, J. Moyer, M.A. Sussman, and V.M. Fowler. 2008. Tropomodulin1 is required in the heart but not the yolk sac for mouse embryonic development. *Circ. Res.* 103:1241–1248. doi:10.1161/CIRCRESAHA.108.178749

Mohandas, N., and E. Evans. 1994. Mechanical properties of the red cell membrane in relation to molecular structure and genetic defects. *Annu. Rev. Biophys. Biomol. Struct.* 23:787–818. doi:10.1146/annurev.bb.23.060194.004035

Mohandas, N., and P.G. Gallagher. 2008. Red cell membrane: past, present, and future. *Blood.* 112:3939–3948. doi:10.1182/blood-2008-07-161166

Moorthy, S., L. Chen, and V. Bennett. 2000. Caenorhabditis elegans beta-G spectrin is dispensable for establishment of epithelial polarity, but essential for muscular and neuronal function. *J. Cell Biol.* 149:915–930. doi:10.1083/jcb.149.4.915

Moré, M.I., F.P. Kirsch, and F.G. Rathjen. 2001. Targeted ablation of NrCAM or ankyrin-B results in disorganized lens fibers leading to cataract formation. *J. Cell Biol.* 154:187–196. doi:10.1083/jcb.200104038

Nelson, W.J., B.L. Granger, and E. Lazarides. 1983. Avian lens spectrin: subunit composition compared with erythrocyte and brain spectrin. *J. Cell Biol.* 97:1271–1276. doi:10.1083/jcb.97.4.1271

Pawley, J.B. 2006. Handbook of Biological Confocal Microscopy. Third edition. Plenum Press, New York. 985 pp.

Pilot, F., and T. Lecuit. 2005. Compartmentalized morphogenesis in epithelia: from cell to tissue shape. *Dev. Dyn.* 232:685–694. doi:10.1002/dvdy.20334

Pollard, T.D., L. Blanchoin, and R.D. Mullins. 2000. Molecular mechanisms controlling actin filament dynamics in nonmuscle cells. *Annu. Rev. Biophys. Biomol. Struct.* 29:545–576. doi:10.1146/annurev.biophys.29.1.545

Praitis, V., E. Ciccone, and J. Austin. 2005. SMA-1 spectrin has essential roles in epithelial cell sheet morphogenesis in C. elegans. *Dev. Biol.* 283:157–170. doi:10.1016/j.ydbio.2005.04.002

Rafferty, N.S. 1985. Lens morphology. *In* The Ocular Lens: Structure, Function, and Pathology. H. Maisel, editor. Marcel Dekker, Inc., New York and Basel. 1–60.

Rao, P.V., and R. Maddala. 2006. The role of the lens actin cytoskeleton in fiber cell elongation and differentiation. *Semin. Cell Dev. Biol.* 17:698–711. doi:10.1016/j.semcdb.2006.10.011

Rauzi, M., P. Verant, T. Lecuit, and P.F. Lenne. 2008. Nature and anisotropy of cortical forces orienting *Drosophila* tissue morphogenesis. *Nat. Cell Biol.* 10:1401–1410. doi:10.1038/ncb1798

Sandilands, A., A.R. Prescott, A. Wegener, R.K. Zoltoski, A.M. Hutcheson, S. Masaki, J.R. Kuszak, and R.A. Quinlan. 2003. Knockout of the intermediate filament protein CP49 destabilises the lens fibre cell cytoskeleton and decreases lens optical quality, but does not induce cataract. *Exp. Eye Res.* 76:385–391. doi:10.1016/S0014-4835(02)00330-5

Sandilands, A., X. Wang, A.M. Hutcheson, J. James, A.R. Prescott, A. Wegener, M. Pekny, X. Gong, and R.A. Quinlan. 2004. Bfsp2 mutation found in mouse 129 strains causes the loss of CP49′ and induces vimentin-dependent changes in the lens fibre cell cytoskeleton. *Exp. Eye Res.* 78:875–889. doi:10.1016/j.exer.2003.09.028

Schevzov, G., B. Vrhovski, N.S. Bryce, S. Elmir, M.R. Qiu, G.M. O'neill, N. Yang, N.M. Verrills, M. Kavallaris, and P.W. Gunning. 2005. Tissue-specific tropomyosin isoform composition. *J. Histochem. Cytochem.* 53:557–570. doi:10.1369/jhc.4A6505.2005

Simirskii, V.N., R.S. Lee, E.F. Wawrousek, and M.K. Duncan. 2006. Inbred FVB/N mice are mutant at the cp49/Bfsp2 locus and lack beaded filament proteins in the lens. *Invest. Ophthalmol. Vis. Sci.* 47:4931–4934. doi:10.1167/iovs.06-0423

Sivak, J.G., K.L. Herbert, K.L. Peterson, and J.R. Kuszak. 1994. The interrelationship of lens anatomy and optical quality. I. Non-primate lenses. *Exp. Eye Res.* 59:505–520. doi:10.1006/exer.1994.1137

Straub, B.K., J. Boda, C. Kuhn, M. Schnoelzer, U. Korf, T. Kempf, H. Spring, M. Hatzfeld, and W.W. Franke. 2003. A novel cell-cell junction system: the cortex adhaerens mosaic of lens fiber cells. *J. Cell Sci.* 116:4985–4995. doi:10.1242/jcs.00815

Sussman, M.A., J.W. McAvoy, M. Rudisill, B. Swanson, G.E. Lyons, L. Kedes, and J. Blanks. 1996. Lens tropomodulin: developmental expression during differentiation. *Exp. Eye Res.* 63:223–232. doi:10.1006/exer.1996.0111

Sussman, M.A., S. Welch, N. Cambon, R. Klevitsky, T.E. Hewett, R. Price, S.A. Witt, and T.R. Kimball. 1998. Myofibril degeneration caused by tropomodulin overexpression leads to dilated cardiomyopathy in juvenile mice. *J. Clin. Invest.* 101:51–61. doi:10.1172/JCI1167

Tardieu, A. 1988. Eye lens proteins and transparency: from light transmission theory to solution X-ray structural analysis. *Annu. Rev. Biophys. Biophys. Chem.* 17:47–70. doi:10.1146/annurev.bb.17.060188.000403

Thomas, G.H. 2001. Spectrin: the ghost in the machine. *Bioessays.* 23:152–160. doi:10.1002/1521-1878(200102)23:2<152::AID-BIES1022>3.0.CO;2-1

Weber, G.F., and A.S. Menko. 2006. Actin filament organization regulates the induction of lens cell differentiation and survival. *Dev. Biol.* 295:714–729. doi:10.1016/j.ydbio.2006.03.056

Weber, A., C.R. Pennise, G.G. Babcock, and V.M. Fowler. 1994. Tropomodulin caps the pointed ends of actin filaments. *J. Cell Biol.* 127:1627–1635. doi:10.1083/jcb.127.6.1627

Weber, K.L., R.S. Fischer, and V.M. Fowler. 2007. Tmod3 regulates polarized epithelial cell morphology. *J. Cell Sci.* 120:3625–3632. doi:10.1242/jcs.011445

Woo, M.K., and V.M. Fowler. 1994. Identification and characterization of tropomodulin and tropomyosin in the adult rat lens. *J. Cell Sci.* 107:1359–1367.

Yoon, K.H., T. Blankenship, B. Shibata, and P.G. Fitzgerald. 2008. Resisting the effects of aging: a function for the fiber cell beaded filament. *Invest. Ophthalmol. Vis. Sci.* 49:1030–1036. doi:10.1167/iovs.07-1149

Zallen, J.A. 2007. Planar polarity and tissue morphogenesis. *Cell.* 129:1051–1063. doi:10.1016/j.cell.2007.05.050

Zelenka, P.S. 2004. Regulation of cell adhesion and migration in lens development. *Int. J. Dev. Biol.* 48:857–865. doi:10.1387/ijdb.041871pz